Cross Sections for Collisions of Electrons and Photons with Oxygen Molecules

Y. Itikawa, A. Ichimura, K. Onda, K. Sakimoto, and K. Takayanagi

Institute of Space and Astronautical Science, Yoshinodai, Sagamihara-shi 229, Japan

Y. Hatano

Department of Chemistry, Tokyo Institute of Technology, Ookayama, Meguroku, Tokyo 152, Japan

M. Hayashi

Nagoya Institute of Technology, Gokiso-cho, Showaku, Nagoya 466, Japan

H. Nishimura

Department of Physics, Niigata University, Igarashi, Niigata 950-21, Japan

S. Tsurubuchi

Department of Applied Physics, Tokyo University of Agriculture and Technology, Koganeishi, Tokyo 184, Japan

Received February 11, 1988; revised manuscript received June 13, 1988

Data have been compiled on the cross sections for collisions of electrons and photons with oxygen molecules (O_2). For electron collisions, the processes included are: total scattering, elastic scattering, momentum transfer, excitations of rotational, vibrational, and electronic states, dissociation, ionization, and attachment. Ionization and dissociation processes are considered for photon impact. Cross-section data selected are presented graphically. Spectroscopic and other properties of the oxygen molecule are summarized for understanding of the collision processes. The literature was surveyed through August 1987, but some more recent data are included when available to the authors.

Key words: cross section data, electron collision, molecular properties, oxygen molecule, photodissociation, photoionization.

Contents

List of Tables

List of Figures

1. Introduction

Oxygen molecules are one of the major components of the Earth's atmosphere. They play an important role also in the atmospheres of other planets. Oxygen is an essential ingredient in various gaseous discharge processes like ozone formation. Collisions of electrons and photons with oxygen molecules, therefore, are fundamental processes in a large number of research areas. The present paper gives the data compiled for those collision processes. A brief summary of the spectroscopic and other properties of oxygen molecules is presented to facilitate the understanding of the collision data. This paper is an extension of a previous report on nitrogen molecules.[1]

The literature has been surveyed through August 1987, but some more recent data available to the present authors are considered. The principle and detailed procedure of compilation and evaluation of the data are essentially the same as in the previous work on nitrogen. The present compilation is based on experimental data. When reliable calculations are available, they are compared with experiment. In a few cases, where a large number of data are reported, the best values determined are presented. In many other cases, where it is difficult to determine which data are better, multi-

ple sets of data are presented. The disagreement among them indicates the degree of their reliability.

As in the previous work, the present compilation has the following restrictions. Collision processes considered here are only those with the oxygen molecule in its electronic ground state. Collisions with molecular ions are excluded, though some spectroscopic data are presented for O_2^+. No data are presented on the angular dependence of the cross section (i.e., the cross section differential with respect to scattering angles). The energy of electrons and photons is limited, in general, to less than 1 keV.

For electron collisions, an attempt is often made to deduce a comprehensive set of cross sections from an analysis of swarm experiments.[2] For instance, Phelps and his collaborators have published several reports of cross sections for O_2 (Phelps[2] and references therein). They are very useful, but the present compilation relies mostly on more direct information from results of beam-type measurements. When compared with the previous case of nitrogen, the number of reliable beam experiments on oxygen is small. The lack of beam data could be compensated with the result of swarm analysis. In order to keep the uniformity of the quality of the data presented, however, such a mixed policy is not taken here.

No detailed discussions about the physics of the collision processes are included in the present paper. They can be found in the original papers cited and in review articles or books (e.g., Christophorou[59]; Shimamura and Takayanagi[60]; Märk and Dunn[61]; Pitchford *et al.*[62]).

In Sec. 2 properties of the oxygen molecule are summarized. In Sec. 3, photon collisions are discussed. In Secs. 4–9, data on electron collisions are presented. Finally, Sec. 10 gives a summary and future problems. Most of the cross section data are presented only in a graphical form. Tables of those data are available upon request to the authors.

2. Properties of the Oxygen Molecule

2.1. Energy Levels

Energy levels and molecular constants were critically surveyed by Krupenie.[3] Spectroscopic constants are summarized also by Huber and Herzberg.[4] There are small differences in the data compiled by the two groups, in both nomenclature and numerical values. Tables 2.1 and 2.2 show the major states of O_2 and O_2^+, respectively. They are selected from the compilation by Krupenie, unless otherwise stated.

The ionization energy of O_2^+ has been determined by several authors. Using the charge transfer reaction, for example, Agee *et al.*[5] obtained the value of 36.1 ± 1.0 eV. This

TABLE 2.1 Major electronic states of O_2 (All values are taken from the review by Krupenie[a,r] unless otherwise stated in the footnotes).

State	T_0[b] (eV)	Diss. products[c]	D^0[d] (eV)	$\Delta E_{vib}(0-1)$[e] (eV)	B_0[f] (10^{-4} eV)	r_e[g] (Å)	Footnote
$a\,^1\Sigma_u^+$	9.455			0.234	2.097	1.11_3[h]	i
$\beta\,^3\Sigma_u^+$	9.355			0.238	2.1	1.10_4[h]	j
$e(^1\Delta_{2u})$	9.346			0.227	2.085	1.119	h
$e'(^3\Delta_{2u})$	9.318			0.254			h
$d(^1\Pi_g)$	8.595			0.231			h
$^3\Pi_g$	8.141			0.228			h,k
$B\,^3\Sigma_u^-$	6.120	$(^3P_g + {}^1D_g)P_r$	0.963	0.0853	1.008	1.6043	
$A\,^3\Sigma_u^+$	4.340[l]	$^3P_g + {}^3P_g$	0.775	0.0961[l]	1.121[l]	1.5215[l]	
$C\,^3\Delta_u$	4.262[m]	$^3P_g + {}^3P_g$	0.861	0.0983[m,n]	1.117[m]	1.527[m]	o
$c\,^1\Sigma_u^-$	4.050[p]	$^3P_g + {}^3P_g$	1.066	0.0954[p]	1.125[p]	1.518[p]	
$b\,^1\Sigma_g^+$	1.627	$^3P_g + {}^3P_g$	3.489	0.174	1.725	1.2268	
$a\,^1\Delta_g$	0.977	$^3P_g + {}^3P_g$	4.138	0.184[q]	1.758	1.2157	
$X\,^3\Sigma_g^-$	0	$^3P_g + {}^3P_g$	5.116	0.193	1.783	1.2075	

[a]Energy units are changed with the conversion factor $1\ \text{cm}^{-1} = 1.239\,85 \times 10^{-4}$ eV.
[b]Energy of the lowest vibrational state relative to $O_2\ X\,^3\Sigma_g^-\ (v=0)$.
[c]Electronic states of the dissociation products, O + O. The states with P_r can predissociate.
[d]Dissociation energy.
[e]Energy difference between the vibrational states with $v=0$ and 1.
[f]Rotational constant for the lowest vibrational state ($v=0$).
[g]Equilibrium internuclear distance.
[h]Taken from Huber and Herzberg (Ref. 4).
[i]Huber and Herzberg (Ref. 4) identify this state as $f\,^1\Sigma_u^+$.
[j]Huber and Herzberg (Ref. 4) identify this state as $D\,^3\Sigma_u^+$.
[k]Huber and Herzberg (Ref. 4) identify this state as $C(^3\Pi_g)$.
[l]Taken from Borrell, Borrell, and Ramsay (Ref. 115).
[m]Taken from Coquart and Ramsay (Ref. 116).
[n]Huber and Herzberg (Ref. 4) give $\Delta E_{vib}(0-1) = 0.100$ eV.
[o]Huber and Herzberg (Ref. 4) identify this state $A'\,^3\Delta_u$.
[p]Taken from Ramsay (Ref. 117).
[q]Huber and Herzberg (Ref. 4) give $\Delta E_{vib}(0-1) = 0.181$ eV.
[r]Ref. 3.

TABLE 2.2. Major electronic states of O_2^+ (All values are taken from the review by Krupenie[a,p] unless otherwise stated in the footnotes).

State	T_0[b] (eV)	Diss. products[c]	D^0[d] (eV)	$\Delta E_{vib}(0-1)$[e] (eV)	B_0[f] (10^{-4} eV)	r_e[g] (Å)	Footnote
$c\,^4\Sigma_u^-$	24.561			0.191	1.930	1.162[h]	
$(^2\Pi_u)$	23.112						h
[q]	21.325						
$B\,^2\Sigma_g^-$	20.297	$^3P_g + {}^2D_u$	1.761	0.1379		1.298[h]	
$C\,^2\Delta_g$	19.676	$^3P_g + {}^2D_u$	2.381	0.111[h]		1.33[h]	i
$(^2\Phi_u)$	18.657			0.112[h]			h,j
$b\,^4\Sigma_g^-$	18.171	$^1D_g + {}^4S_u$	2.530	0.1442	1.582	1.2797	
$b'(^4\Pi_g)$	17.905						h
$A\,^2\Pi_u$	17.040	$^3P_g + {}^4S_u$	1.694	0.1080	1.305	1.4082[k]	l
$a\,^4\Pi_{ui}$	16.104	$^3P_g + {}^4S_u$	2.629	0.1258	1.360	1.3816	
$X\,^2\Pi_g$	12.072[o]	$^3P_g + {}^4S_u$	6.662	0.2322	2.082[m]	1.1171[n]	

[a]Energy units are changed with the conversion factor 1 $cm^{-1} = 1.239\,85 \times 10^{-4}$ eV.
[b]Energy of the lowest vibrational state relative to $O_2\,X\,^3\Sigma_g(v=0)$.
[c]Electronic states of the dissociation products, $O + O^+$.
[d]Dissociation energy.
[e]Energy difference between the vibrational states with $v=0$ and 1.
[f]Rotational constant for the lowest vibrational state ($v=0$).
[g]Equilibrium internuclear distance.
[h]Taken from Huber and Herzberg (Ref. 4).
[i]Huber and Herzberg (Ref. 4) identify this state as $D\,^2\Delta_g$, and give $T_0 = 19.788$ eV.
[j]Huber and Herzberg (Ref. 4) identify this state as $C\,^2\Phi_u$.
[k]Huber and Herzberg (Ref. 4) give $r_e = 1.4091$ Å.
[l]Huber and Herzberg (Ref. 4) give $T_0 = 17.051$ eV.
[m]Huber and Herzberg (Ref. 4) give $B_0 = 2.085 \times 10^{-4}$ eV.
[n]Huber and Herzberg (Ref. 4) give $r_e = 1.1164$ Å.
[o]Ionization energy of O_2.
[p]Reference 3.
[q]Unknown state.

is consistent with the data previously reported (see Agee *et al.*[5]).

Theoretical studies of the potential curves for O_2, O_2^+, and O_2^{2+} have been made by many people. Detailed calculations are reported, for instance, by Beebe *et al.*,[6] Saxon and Liu[7,8] and Michels.[9]

There are a large number of determinations of the electron affinity (EA) of O_2 (see a review of Christodoulides *et al.*[10]). Celotta *et al.*[11] obtained

$$\mathrm{EA}(O_2) = 0.440 \pm 0.008 \text{ eV} \tag{2.1}$$

from a detailed energy analysis of the electrons photodetached from O_2^-. Most of the other recent measurements confirmed this result (see Christodoulides *et al.*[10]). Some other spectroscopic constants of O_2^- are listed in Table 2.3. Little experimental work on the excited states of O_2^- has been published. Das *et al.*[12] calculated the potential energy curves for several excited states of O_2^-.

TABLE 2.3. Spectroscopic constants for $X\,^2\Pi_g$ state of O_2^-.

D^0	4.09 ± 0.01 eV[a]
$\Delta E_{vib}(0 \to 1)$	0.133 eV[b]
B_e	$(1.45 \pm 0.02) \times 10^{-4}$ eV[a]
r_e	1.341 ± 0.010 Å[a]

[a] Celotta *et al.* (Ref. 11).
[b] Linder and Schmidt (Ref. 75).

2.2. Molecular Properties

Oxygen has isotopes of mass 16, 17, and 18, but the most abundant naturally occurring oxygen molecule is $^{16}O_2$. The mass of $^{16}O_2$ is

$$M = 5.312\,12 \times 10^{-23} \text{ g}, \tag{2.2}$$

which gives the mass ratio

$$m_e/M = 1.7149 \times 10^{-5} \tag{2.3}$$

(m_e being the electron mass).

The oxygen molecule has an electric quadrupole and higher multipole moments. With the use of far-IR collision-induced absorption, Birnbaum and Cohen[13] determined the quadrupole q and the hexadecupole Φ moments as follows:

$$q = -0.35 \times 10^{-26} \text{ esu cm}^2, \tag{2.4}$$

$$\Phi = 3.3 \times 10^{-42} \text{ esu cm}^4. \tag{2.5}$$

The polarizability of O_2 has two components: $\alpha_\parallel$ and $\alpha_\perp$. The quantity $\alpha_\parallel$ ($\alpha_\perp$) denotes the polarization induced by a field parallel (perpendicular) to the molecular axis. From the distribution of dipole oscillator strengths, Zeiss and Meath[14] determined the best value of the isotropic part of the polarizability as

$$\alpha_0 = \tfrac{1}{3}(\alpha_\parallel + 2\alpha_\perp) = 1.569 \times 10^{-24} \text{ cm}^3. \tag{2.6}$$

Buldakov *et al.*[15] obtained the anisotropy of the polarizability

$$\gamma = \alpha_{\parallel} - \alpha_{\perp}$$
$$= 1.12\times10^{-24}\ \text{cm}^3 . \quad (2.7)$$

The same group[16] also determined the derivative of the polarizability at the equilibrium internuclear distance

$$\left(\frac{d\alpha_0}{dR}\right)_{R=r_e} = 1.46\times10^{-16}\ \text{cm}^2 , \quad (2.8)$$

$$\left(\frac{d\gamma}{dR}\right)_{R=r_e} = 2.64\times10^{-16}\ \text{cm}^2 . \quad (2.9)$$

2.3. Oscillator Strengths and Lifetimes for Bound–Bound Transitions

The Schumann-Runge absorption bands due to the transition $B\,^3\Sigma_u^- - X\,^3\Sigma_g^-$ have been studied by many people. Table 2.4 shows two recent determinations of the absorption oscillator strengths for the Schumann–Runge bands. The band oscillator strength depends on the gaseous temperature through the population of the rotational states of O_2. The Harvard group[17,18] made a very high resolution measurement and directly integrated the absorption cross sections for each rotational line. The Australian group[19] determined the oscillator strength of individual rotational lines on the basis of the high-resolution measurement and an equivalent width analysis. They first derived the rotational-state dependence of the oscillator strength and then averaged over the rotational population. Both the measurements were made at 300 K. The agreement between the two sets of the data shown in Table 2.4 is quite good. Very recently Yoshino *et al.*[20] reported their measurement at 79 K. The absorption from higher vibrational states has been also studied. Some results are shown in Table 2.5.

TABLE 2.4. Absorption oscillator strengths for the Schumann–Runge bands of O_2 ($B\,^3\Sigma_u^- v'$–$X\,^3\Sigma_g^- v'' = 0$).

		$f_{v'v''}$	
v'	λ (nm)	Yoshino *et al.*[a]	Lewis *et al.*[b]
0	202.593	$2.95 \pm 0.15\ (-10)$[c]	
1	199.817	$3.13 \pm 0.16\ (-9)$	$3.04 \pm 0.15\ (-9)$
2	197.197	$1.89 \pm 0.19\ (-8)$	$1.94 \pm 0.06\ (-8)$
3	194.733	$8.45 \pm 0.42\ (-8)$	$8.14 \pm 0.25\ (-8)$
4	192.419	$2.82 \pm 0.14\ (-7)$	$2.74 \pm 0.09\ (-7)$
5	190.254	$7.42 \pm 0.37\ (-7)$	$7.42 \pm 0.25\ (-7)$
6	188.243	$1.62 \pm 0.08\ (-6)$	$1.67 \pm 0.05\ (-6)$
7	186.372	$3.43 \pm 0.17\ (-6)$	$3.44 \pm 0.11\ (-6)$
8	184.651	$6.31 \pm 0.32\ (-6)$	$6.08 \pm 0.20\ (-6)$
9	183.076	$1.00 \pm 0.05\ (-5)$	$9.65 \pm 0.30\ (-6)$
10	181.650	$1.54 \pm 0.08\ (-5)$	$1.47 \pm 0.05\ (-5)$
11	180.379	$2.26 \pm 0.11\ (-5)$	$1.96 \pm 0.06\ (-5)$
12	179.261	$2.43 \pm 0.12\ (-5)$	$2.44 \pm 0.08\ (-5)$
13	178.3		$2.73 \pm 0.09\ (-5)$
14	177.5		$2.82 \pm 0.10\ (-5)$
15	176.8		$2.73 \pm 0.10\ (-5)$
16	176.3		$2.63 \pm 0.10\ (-5)$
17	175.9		
18	175.6		
19	175.4		
20	175.2		

[a] Yoshino *et al.* (Ref. 17), supplemented with the values for $v' = 0$ and 1 from Cheung *et al.* (Ref. 18).
[b] Lewis *et al.* (Ref. 19).
[c] $2.95\ (-10) = 2.95\times10^{-10}$.

TABLE 2.5. Absorption oscillator strengths for the Schumann–Runge bands of O_2 ($B\,^3\Sigma_u^- v' - X\,^3\Sigma_g^- v''$) from the excited vibrational states.

	$v'' = 1$[a]		$v'' = 2$[b]	
v'	λ (nm)	$f_{v'v''}$	λ (nm)	$f_{v'v''}$
0				
1				
2				
3	200.7	$1.76 \pm 0.12\ (-6)$[c]		
4	198.4	$5.03 \pm 0.25\ (-6)$		
5	196.1	$1.24 \pm 0.07\ (-5)$		
6	193.9	$2.68 \pm 0.14\ (-5)$	199.9	$2.13\ (-4)$
7	191.9	$5.03 \pm 0.25\ (-5)$	197.8	$3.39\ (-4)$
8	190.1	$8.57 \pm 0.40\ (-5)$	195.8	$5.46\ (-4)$
9	188.5	$1.20 \pm 0.10\ (-4)$	194.1	$9.87\ (-4)$
10	186.9	$1.71 \pm 0.10\ (-4)$	192.5	$1.03\ (-3)$
11	185.6	$2.05 \pm 0.10\ (-4)$	191.0	$1.04\ (-3)$
12	184.4	$2.61 \pm 0.14\ (-4,$	189.8	$1.22\ (-3)$
13	183.4	$2.58 \pm 0.30\ (-4)$	188.7	$1.04\ (-3)$
14	182.5	$2.93 \pm 0.30\ (-4)$		
15	181.8	$2.52 \pm 0.20\ (-4)$		
16	181.3	$2.09 \pm 0.25\ (-4)$		

[a] Lewis *et al.* (Ref. 19).
[b] Hudson and Carter (Ref. 118).
[c] $1.76\ (-6) = 1.76\times10^{-6}$.

The $B\,^3\Sigma_u^-$ state of O_2 is well known to predissociate. The rate of predissociation is reflected in the width of each rotational line of the Schumann–Runge bands. A number of measurements have been reported on the linewidths. Table 2.6 gives the result of recent experimental work of very high resolution.[21] They obtained the width of individual rotational lines. The values in Table 2.6 are the widths extrapolated to zero rotation. They derived an empirical formula to evaluate the linewidth of any rotational–vibrational line with $v = 0$–21 and $J \leqslant 40$.

Another important absorption in O_2 is the Herzberg I bands ($A\,^3\Sigma_u^+ X\,^3\Sigma_g^-$). Two sets of measurements of the

TABLE 2.6. Predissociation linewidths (in cm^{-1}) for the Shumann–Runge bands of O_2 (Lewis *et al.*[a]).

v	Linewidth (cm^{-1})
1	0.66 ± 0.10
2	0.39 ± 0.03
3	1.61 ± 0.08
4	2.99 ± 0.20
5	1.91 ± 0.10
6	1.38 ± 0.10
7	1.87 ± 0.10
8	1.61 ± 0.10
9	0.67 ± 0.05
10	0.95 ± 0.05
11	1.18 ± 0.10
12	0.42 ± 0.05
13	0.11 ± 0.01
14	0.18 ± 0.02
15	0.33 ± 0.03
16	0.35 ± 0.05
17	0.34 ± 0.03
18	0.22 ± 0.03
19	0.23 ± 0.04

[a] Reference 21.

TABLE 2.7. Absorption oscillator strengths for the Herzberg I bands of O_2 ($A\,^3\Sigma_u^+ v' - X\,^3\Sigma_g^- v'' = 0$).

		$f_{v'v''}$	
v'	λ (nm)	a	b
0	(285.6)	8.47 (− 14)[c]	
1	279.4	7.39 (− 13)	
2	273.7	3.31 (− 12)	
3	268.5	1.02 (− 11)	
4	263.7	2.44 (− 11)	3.0 (− 11) ± 20%
5	259.3	4.84 (− 11)	5.38 (− 11) ± 15%
6	255.4	8.29 (− 11)	7.98 (− 11) ± 15%
7	251.9	1.23 (− 10)	1.24 (− 10) ± 15%
8	248.9	1.62 (− 10)	1.39 (− 10) ± 15%
9	246.3	1.84 (− 10)	1.4 (− 10) ± 20%
10	244.3	1.76 (− 10)	1.2 (− 10) ± 20%
11	242.9	1.25 (− 10)	1.0 (− 10) ± 30%

[a] The relative measurement by Degen and Nicholls (Ref. 119), normalized to the absolute value at $(v',v'') = (7,0)$ obtained by Hasson *et al.* (Ref. 120).
[b] Hasson and Nicholls (Ref. 121).
[c] $8.47\,(-14) = 8.47\times10^{-14}$.

absorption oscillator strength for the bands are shown in Table 2.7.

The probabilities of the transitions from the states $a\,^1\Delta_g$ and $b\,^1\Sigma_g^+$ are summarized by Krupenie.[3] His results are reproduced in Table 2.8 for the reader's convenience. Krupenie compiled also the tables of the Franck–Condon factors for the bound–bound transitions in O_2 and O_2^+.

Table 2.9 shows the experimental data of the lifetimes of the states $A\,^2\Pi_u$ and $b\,^4\Sigma_g^-$ of O_2^+.[22] Those states decay mainly through the second negative ($A\,^2\Pi_u \rightarrow X\,^2\Pi_g$) and the first negative ($b\,^4\Sigma_g^- \rightarrow a\,^4\Pi_u$) transitions, respectively. Fink and Welge[23] also reported their measurement of those lifetimes but only for a few vibrational levels. Their results agree with the values in Table 2.9 within the error limit. For the lifetime of the state $A\,^2\Pi_u$, Wetmore *et al.*[24] made a detailed calculation over the vibrational levels up to $v' = 33$, but their absolute magnitudes are somewhat larger than the measured values. The higher vibrational states ($v' \geqslant 5$) of the state $b\,^4\Sigma_g^-$ can predissociate. The rate of predissociation was measured by Moseley *et al.*[25] and Hansen *et al.*[26]

Because of the triplet spin state, the oxygen molecule in its electronic ground state has a strong magnetic dipole moment. This causes a magnetic dipole transition among different (N, J) states, where N is rotational quantum number and J is total angular momentum quantum number. Those transitions give rise to the emission or absorption of radiation in the mm to IR region. Black and Smith[27] studied the transition in some detail in relation to the detectability of interstellar O_2. Laboratory measurements of the absorption were made, for instance, by Boreiko *et al.*[28]

TABLE 2.8. Probability A of the transitions from the states $a\,^1\Delta_g$ and $b\,^1\Sigma_g^+$ of O_2 compiled by Krupenie[a].

Transitions	A (s^{-1})
$a\,^1\Delta_g v' = 0 \rightarrow X\,^3\Sigma_g^- v'' = 0$	2.58×10^{-4}
$b\,^1\Sigma_g^+ v' \rightarrow X\,^3\Sigma_g^- v''$	
$(v',v'') = (0,0)$	0.085
(1,0)	(0.0069)
(2,0)	0.1636×10^{-3}
(3,0)	0.0704
$b\,^1\Sigma_g^+ v' = 0 \rightarrow a\,^1\Delta_g v'' = 0$	1.5×10^{-3}

[a] Reference 3.

TABLE 2.9. Lifetimes (in μs) of the states $A\,^2\Pi_u v'$ and $b\,^4\Sigma_g^- v'$ of O_2^+.[a]

v'	$A\,^2\Pi_u$	$b\,^4\Sigma_g^-$
0	0.677	1.12 ± 0.04
1	0.679	1.10 ± 0.05
2	0.679	1.22 ± 0.04
3	0.666	
4	0.671	
5	0.680	
6	0.675	
7	0.676	

[a] Reference 22.

2.4. Distribution of Dipole Oscillator Strengths and Moments

The distribution of dipole oscillator strengths can be characterized in terms of moments:

$$S(\mu) = \sum_n \left(\frac{E_n}{\mathrm{Ry}}\right)^\mu f_n + \int_{I_1}^\infty \left(\frac{E}{\mathrm{Ry}}\right)^\mu \frac{df}{dE}\,dE \tag{2.10}$$

$$L(\mu) = \sum_n \left(\frac{E_n}{\mathrm{Ry}}\right)^\mu \ln\left(\frac{E_n}{\mathrm{Ry}}\right) f_n + \int_{I_1}^\infty \left(\frac{E}{\mathrm{Ry}}\right)^\mu \ln\left(\frac{E}{\mathrm{Ry}}\right) \frac{df}{dE}\,dE \tag{2.11}$$

$$I(\mu) = \exp[L(\mu)/S(\mu)]\,\mathrm{Ry}\,. \tag{2.12}$$

Here E_n is the excitation energy of the nth state, f_n is the dipole oscillator strength for the transition from the ground to the nth state, df/dE is the density of the oscillator strength per unit energy for continuum excitation, and I_1 is the first ionization potential. All the energies are expressed in rydberg units (1 Ry = 13.61 eV). Zeiss *et al.*[122] determined semiempirically the best values of those moments. Their results are shown in Table 2.10.

TABLE 2.10. Moments of dipole oscillator strengths.[b]

μ	$S(\mu)$	$L(\mu)$	$I(\mu)$ (in eV)
2	8.484(4)[a]	6.096(5)	1.796(4)
1	3.744(2)	1.609(3)	1.001(3)
0	1.600(1)	3.110(1)	9.507(1)
− 1/2	7.509		
− 1	4.652	3.664	2.992(1)
− 3/2	3.336		
− 2	2.648	9.946(− 1)	1.982(1)
− 5/2	2.282		
− 3	2.114		
− 4	2.172		
− 6	3.705		
− 8	8.578		
− 10	2.223(1)		
− 12	6.042(1)		
− 14	1.689(2)		

[a] $8.484(4) = 8.484\times10^4$.
[b] Reference 122.

3. Photoionization and Photodissociation

3.1. Photoionization

3.1. a. Total Cross Section

In 1979, Berkowitz[29] and Kirby *et al.*[30] independently published their recommended data on the photoionization cross section for O_2. Here recommended values are redetermined on the basis of several recent measurements (Cole and Dexter[31] for 5–34 nm; Mehlman *et al.*[32] for 6–34 nm; Brion *et al.*[33] for 16.5–112.7 nm; Samson *et al.*[34] for 12–68.4 nm). Cole and Dexter and Mehlman *et al.* actually measured the photoabsorption cross section (Q^{ph}_{abs}), but in the wavelength range of their experiments, Q^{ph}_{abs} can be assumed the same as the photoionization cross section (Q^{ph}_{ion}).

Cole and Dexter and Mehlman *et al.* used synchrotron radiation as a light source. Samson *et al.* employed a spark discharge. Brion *et al.* determined Q^{ph}_{ion} using the electron-impact method. These four sets of data are in quite good agreement with each other. The best values of Q^{ph}_{ion} for 5–60 nm have been determined by smoothly connecting those data points in that region. The result is shown in Fig. 3.1.

At the wavelengths longer than 60 nm, a complicated structure due to autoionization appears in the wavelength dependence of Q^{ph}_{ion}. As a typical example, Q^{ph}_{ion}, measured by Matsunaga and Watanabe,[35] is presented in Fig. 3.1. They obtained those cross sections with a resolution of 0.02–0.03 nm. To avoid cluttering the figure, their cross section is plotted in Fig. 3.1 only at an interval of ~1.0 nm in the region 60–90 nm. Dehmer and Chupka[36] measured the cross section with a higher resolution (0.007 nm) in the same wavelength region as that studied by Matsunaga and Watanabe. Dehmer and Chupka reported, however, their cross sections only in a relative scale.

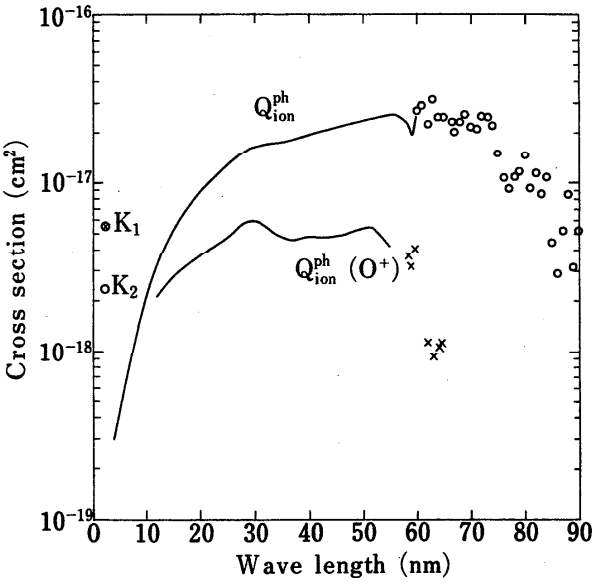

FIG. 3.1. Total (Q^{ph}_{ion}) and dissociative [Q^{ph}_{ion} (O⁺)] photoionization cross sections. At wavelengths longer than 60 nm for Q^{ph}_{ion} and 54 nm for Q^{ph}_{ion} (O⁺), complicated structure due to autoionization and predissociation is apparent. In those regions, only representative data are shown (see the text). Peaks in the K absorption region are indicated by K_1 and K_2.

Near the K-edge [at 543.1 eV ($^4\Sigma$) and 544.2 eV ($^2\Sigma$) for O_2], the ionization cross section is enhanced by a resonance process (LaVilla[37]; Barrus *et al.*[38]). Barrus *et al.* determined the cross section carefully, taking proper account of pressure dependence. Figure 3.1 shows their values of Q^{ph}_{ion} at two prominent peaks, each denoted by K_1 (at 2.34 nm) and K_2 (2.29 nm). Above the threshold of K-shell ioni-

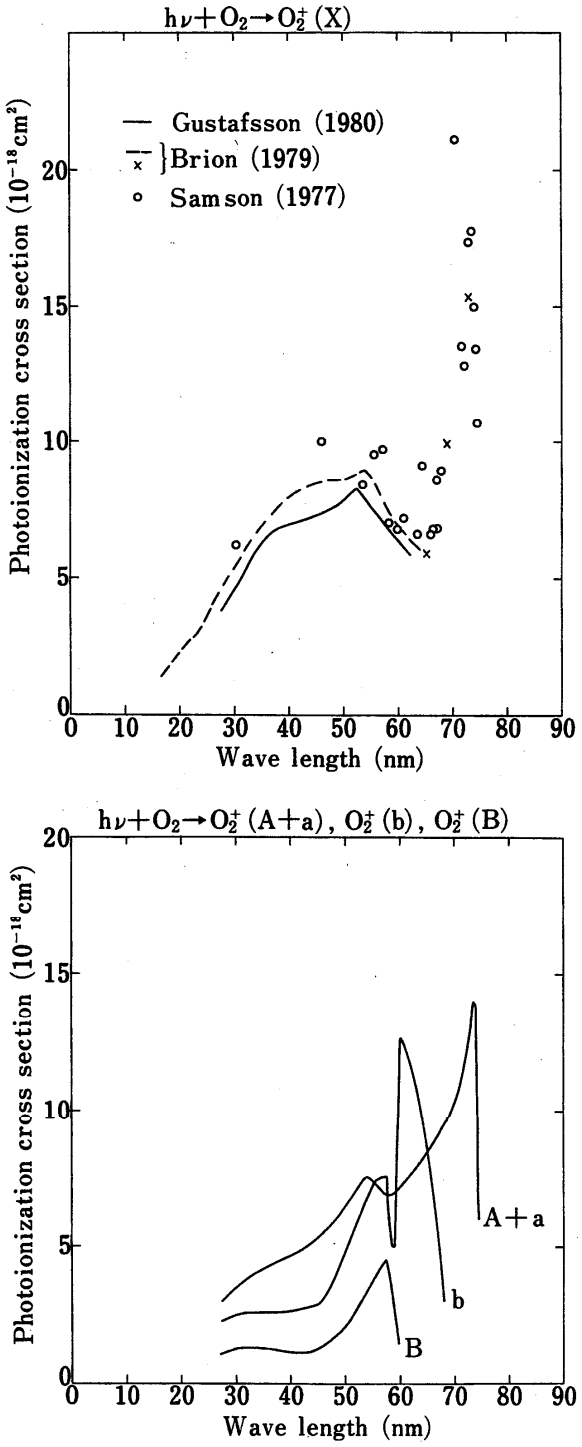

FIG. 3.2. Partial photoionization cross sections for the production of O_2^+ in the states (a) $X\,^2\Pi_g$ and (b) $A\,^2\Pi_u + a\,^4\Pi_u$, $b\,^4\Sigma_g^-$, $B\,^2\Sigma_g^-$.

zation, Bodeur[39] measured Q_{ion}^{ph}, which decreases monotonically from the value of 0.98×10^{-18} cm^2 at 2.2 nm to 0.03×10^{-18} cm^2 at 0.6 nm.

3.1. b. Partial Cross Sections

By using photoelectron spectroscopy, Samson *et al.*[40] and Gustafsson[41] determined the branching ratio for the production of specific states of O_2^+. Upon normalization to their own total photoionization cross section, Samson *et al.* obtained the partial photoionization cross section for several states of O_2^+. Gustafsson reported similar partial cross sections based on the normalization to the total cross section measured by Lee *et al.*[42] Independent of these two experiments, Brion *et al.*[33] determined the partial cross section with the $(e,2e)$ technique and normalization to their own total cross section.

Figure 3.2(a) shows the partial ionization cross section for the production of O_2^+ ($X\,^2\Pi_g$). The three sets of data mentioned above are compared. It should be noted that Gustafsson and Brion *et al.* employed a continuum light source or the equivalent, while Samson *et al.* used line radiation. The amount of disagreement among the three measurements indicates the reliability of those results.

For the production of O_2^+ ($B\,^2\Sigma_g^-$), the results of the above three experiments are in reasonable agreement. Figure 3.2(b) gives those data connected smoothly. The states, $b\,^4\Sigma_g^-$,$a\,^4\Pi_u$,$A\,^2\Pi_u$ are closely located. Brion *et al.* could not resolve them. Gustafsson and Samson *et al.* give the partial cross sections for O_2^+ ($b\,^4\Sigma_g^-$) and O_2^+ ($a\,^4\Pi_u + A\,^2\Pi_u$). Gustafsson obtained the cross section only at photon energies above 20 eV. Figure 3.2(b) presents the cross sections of Gustafsson supplemented with the data of Samson *et al.* at lower energies. In the longer-wave length region (>60 nm), the original data points scatter widely and only the smoothed behavior is shown in Fig. 3.2(b). Gustafsson reported partial photoionization cross sections also for several highly excited states (e.g., $c\,^4\Sigma_u^-$) of O_2^+.

Edqvist *et al.*[43] measured photoelectrons from O_2 with very high resolution at 58.4 nm. From an analysis of their data, they determined the branching ratio of O_2^+ ($a\,^4\Pi_u$) to O_2^+ ($A\,^2\Pi_u$) to be 6.7:1. No information is available for the wavelength dependence of the branching ratio. For the production of O_2^+ ($b\,^4\Sigma_g^-$) and O_2^+ ($B\,^2\Sigma_g^-$), Morin *et al.*[44] made a very detailed experimental study in the region 51–68 nm. Their result is in general agreement with the corresponding cross section shown in Fig. 3.2(b).

Wu *et al.*[45] and Tabche-Fouhaile *et al.*[46] measured the fluorescence upon the photoionization of O_2. Both groups detected the emissions from the transitions $A\,^2\Pi_u \rightarrow X\,^2\Pi_g$ and $b\,^4\Sigma_g^- \rightarrow a\,^4\Pi_u$ upon illumination with 45–75 nm light. Their emission cross sections, however, disagree strongly both in magnitude and in relative wavelength dependence. Probably this is caused by the differences in the collection method of the fluorescence and in the normalization procedure.

3.1. c. Dissociative Ionization

The yield of O^+ at the photoionization of O_2 was measured by Brion *et al.* and Samson *et al.* The cross sections obtained by the two groups for this process, $Q_{ion}^{ph}(O^+)$, are in good agreement with each other. The values connected smoothly are plotted in Fig. 3.1. It should be noted that, at wavelengths shorter than 16 nm, O^+ is produced much more efficiently than O_2^+. In the region of longer wavelength (>54 nm), $Q_{ion}^{ph}(O^+)$ has complicated structure due to autoionization and predissociation. Several typical values of $Q_{ion}^{ph}(O^+)$ in this region[34] are indicated by crosses in Fig. 3.1. Detailed study for that region was made by Dehmer and Chupka[36] and Akahori *et al.*[47]

3.1. d. Production of Ion Pairs: O^+ and O^-

Considering the electron affinity of an oxygen atom, the threshold of the process

$$h\nu + O_2 \rightarrow O^+ + O^-$$

is at 71.781 nm (17.272 eV). There are several groups observing O^- at the photoionization of O_2 (Elder *et al.*[48] for 69–72.5 nm; Dibeler and Walker[49] for 69–72.5 nm; Dehmer and Chupka for 58–72 nm; Oertel *et al.*[50] for 41.3–72.9 nm). None of the authors reported an absolute magnitude of the cross section $Q_{ion}^{ph}(O^-)$ for the production of O^-. They give only the relative dependence of the cross section on the wavelength of the incident light.

The cross section $Q_{ion}^{ph}(O^-)$ has a peak at about 71 nm and decreases sharply as the wavelength decreases. It gradually increases again at ~60 nm and has a second maximum at 57.7 nm. According to Dibeler and Walker, the yield ratio O^-/O_2^+ is about 0.03 at the first peak (at ~71 nm). Oertel *et al.* show that the height ratio of the second peak to the first one is ~0.5. These numbers, however, should not be taken seriously, because the difference in the detection efficiency of each ion is not taken into account in those experiments.

3.2. Photodissociation (Production of Neutral Fragments)

When oxygen molecules absorb photons of the energy above the dissociation threshold (5.12 eV or 242.4 nm), most of them are either dissociated or ionized. Fig. 3.3 shows the absorption cross section Q_{abs}^{ph} for the energy range 130–250 nm. Figure 3.4 gives Q_{abs}^{ph} for 90–130 nm. The cross sections shown in the figures can be regarded as the dissociation cross section Q_{diss}^{ph}, except in the region of the Schumann–Runge bands (175–200 nm) and the region above the ionization threshold (<102.7 nm).

The continuum in the absorption spectrum due to the dissociation process through the excitation of O_2 ($A\,^3\Sigma_u^+$) is called the Herzberg continuum. That region has been extensively studied. (The work up to 1983 is summarized by Cheung *et al.*[18]) This process results in the production of two $O(^3P)$. Owing to the smallness of the cross section, it is very difficult to reliably obtain its absolute magnitude. Jenouvrier *et al.*[51] determined the cross section carefully with a very long path length for absorption and by widely varying the gas pressure. Very recently Cheung *et al.*[52] made a similar measurement but with a somewhat shorter path length. The two results almost coincide with each other within their combined errors. Figure 3.3 shows the cross section obtained

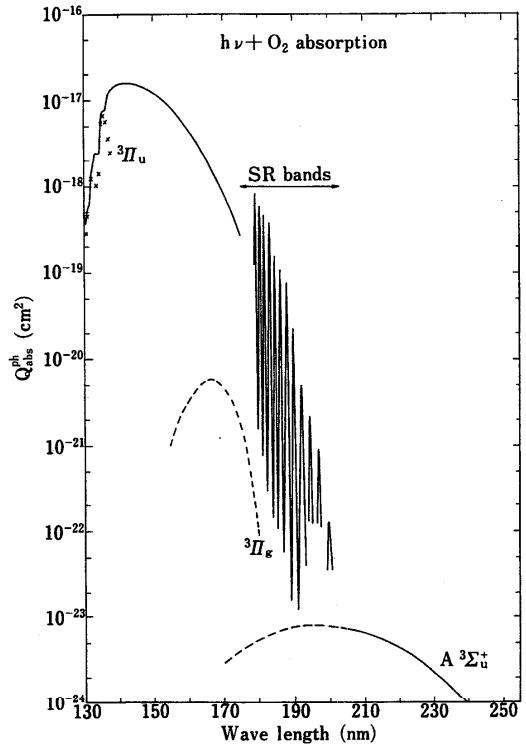

FIG. 3.3. Photoabsorption cross section in the wavelength region 130–250 nm. Dashed line with $^3\Pi_g$ is the contribution due to the excitation of $^3\Pi_g$ state of O_2, estimated by Lewis *et al.*[54] Crosses are the $^3\Pi_u$ excitatoin derived by Lee *et al.*[123]

by Jenouvrier *et al.* Their cross sections are extended to the region of higher energies by fitting to the empirical formula proposed by Johnston *et al.*[53]

The absorption spectrum due to excitation of the $B\,^3\Sigma_u^-$ state of O_2 is divided into two parts: the Schumann–Runge bands (> 175 nm) and the Schumann–Runge continuum (< 175 nm). The latter corresponds to the dissociation $O_2 \rightarrow O(^3P) + O(^1D)$. A part of the photoabsorption in the former region also induces a dissociation of O_2 [$\rightarrow O(^3P) + O(^3P)$] through predissociation (see Sec. 2). As an illustration, Fig. 3.3 shows rather schematically (without rotational structure) the absorption cross sections of the Schumann–Runge bands. They are obtained by Yoshino *et al.*[17] at an instrumental bandwidth of $\sim 0.4\ cm^{-1}$. There is a background continuum underlying the Schumann–Runge bands absorption. Lewis *et al.*[54] analyzed absorption spectra in the region and deduced the cross section for continuum absorption. They attributed the absorption to excitation of the $^3\Pi_g$ state of O_2, which dissociates into $O(^3P) + O(^3P)$. This cross section is also given in Fig. 3.3.

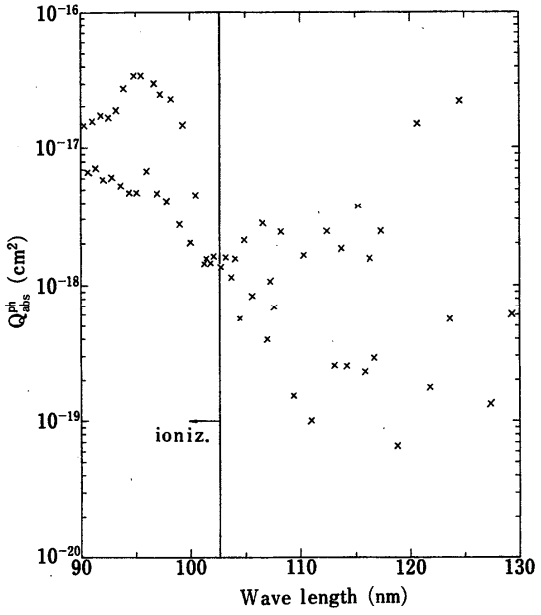

FIG. 3.4. Photoabsorption cross section in the wavelength region 90–130 nm. Only the minimum and maximum values are plotted as determined by Huebner *et al.*[56]

At wavelengths shorter than 175 nm, the absorption cross section was measured very extensively by Ogawa and Ogawa[55] and Huebner *et al.*[56] The latter authors used the electron impact method to obtain the oscillator strength. The two results are in good agreement in the region 130–175 nm. Those cross sections are connected smoothly and shown in Fig. 3.3. At wavelengths shorter than 130 nm, the absorption cross sections vary rapidly so that their values depend strongly on the experimental resolution. As an illustration, Fig. 3.4 presents the Q_{abs}^{ph} of Huebner *et al.* They determined Q_{abs}^{ph} in 10-meV energy loss intervals. In Fig. 3.4, however, only the maximum and minimum values are plotted.

Lee *et al.*[123] measured the quantum yield of O upon photodissociation of O_2 by detecting the chemiluminescence of NO_2 formed in the mixture of O_2, O, and NO. Over the wavelength range considered (116–177 nm), the quantum yield is two, within the experimental error of $\pm$ 20%. This indicates that, in this spectral region, all the photoabsorption leads to dissociation. Lee *et al.* also determined the quantum yield of $O(^1D)$ by measuring emission from the reaction $O(^1D) + O_2$. The yield of $O(^1D)$ was found to be unity in the wavelength region 140–177 nm. Thus, dissociation to $O(^1D) + O(^3P)$ through excitation of O_2 ($B^3\Sigma_u^-$) dominates this region. For incident photons of shorter wavelength, the main process is dissociation into $O(^3P) + O(^3P)$ through excitation of repulsive states, or predissociation of highly excited states of O_2. In particular the yield of $O(^1D)$ decreases almost to zero at around 135 nm. Lee *et al.* ascribed this to excitation of the $^3\Pi_u$ state of O_2. This was theoretically confirmed by Allison *et al.*[57] In Fig. 3.3, the excitation cross section for the state is shown as estimated by Lee *et al.*

Lawrence and McEwan[58] detected emission from $O(^1S)$ upon photodissociation of O_2 in the region 85–130 nm. The quantum yield of $O(^1S)$ is small and has a maximum value of ~ 0.1 at 105 nm.

Above the ionization threshold, the ionization yield, η_{ion} ($= Q_{ion}^{ph}/Q_{abs}^{ph}$), has been measured several times. The measurements show η_{ion} to be unity for wavelengths shorter than 62 nm (e.g., Berkowitz[29]). In the longer-wavelength region, we have $\eta_{ion} < 1$ but the difference $Q_{abs}^{ph} - Q_{ion}^{ph}$ is not necessarily equal to Q_{diss}^{ph}. Some part of the absorption results in excitation of Rydberg states of the molecule. Matsunaga and Watanabe estimated Q_{diss}^{ph} from the continuum part of $Q_{abs}^{ph} - Q_{ion}^{ph}$. The result is shown in Fig. 3.5. They

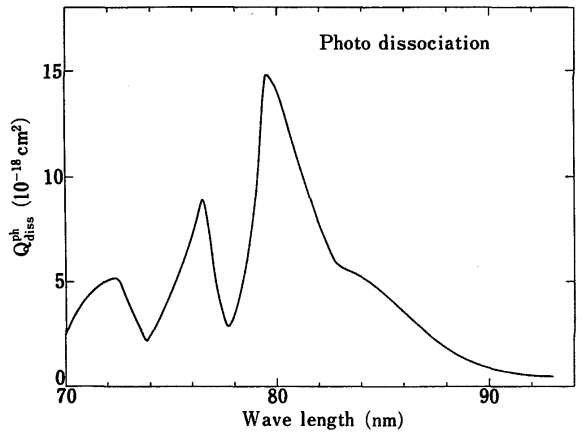

FIG. 3.5. Photodissociation cross section in the wavelength region 70–92 nm, determined by Matsunaga and Watanabe.[35]

concluded that dissociation is almost negligible outside of the wavelength region shown in the figure (<68 nm and >92 nm). Carlson[63] observed fluorescence due to the transition O $2p^3 3s\ ^3S \rightarrow 2p^4\ ^3P$ and O $2p^3 3p\ ^5P \rightarrow 2p^3 3s\ ^5S^0$ upon photodissociation of O_2 in the region 50–90 nm. From the result, he concluded that the peak of Q_{diss}^{ph} shown around 76 nm in Fig. 3.5 is mostly formed by production of $O(2p^3 3p\ ^5P) + O(^3P)$ and $O(2p^3 3p\ ^3P) + O(^3P)$.

Lee *et al.*[64] measured the VUV fluorescence from atomic oxygen produced by photodissociation of O_2. They used synchrotron radiation as the source of incident light in the region 17.5–78 nm. They determined the emission cross section for fluorescence in the region 124–180 nm (mostly from the transition O $2p^3 3s^3S^0 \rightarrow 2p^4\ ^3P$), and that for 105–124 nm (from the transitions $2p^3 3s''\ ^1P^0 \rightarrow 2p^4\ ^1S$ and $2p^3 3s'\ ^1D^0 \rightarrow 2p^4\ ^1D$).

4. Electron Collisions: Total-Scattering, Elastic, and Momentum-Transfer Cross Sections

4.1. Total Scattering Cross Section

In 1981, Hayashi[65] surveyed available data and determined the best values of the total scattering cross section Q_T. His values are based on measurements by Brüche,[66] Ramsauer and Kollath,[67] Sunshine *et al.*,[68] Salop and Nakano,[69] Dehmel *et al.*,[70] and Dalba *et al.*[71] Hayashi adjusted the original data within the experimental errors so that the resulting cross sections are consistent with each other. Recently Zecca *et al.*[72] made a detailed measurement of Q_T for electron energies of 0.2–100 eV. With those recent data taken into account, Hayashi's values have been revised. The result is shown in Fig. 4.1. The accuracy of the present data is $\sim 5\%$.

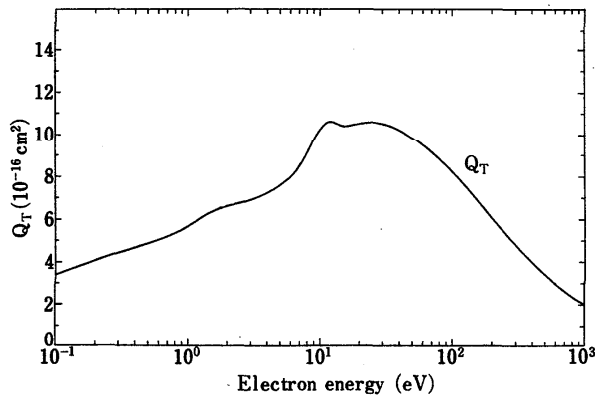

FIG. 4.1. Total cross section for electron scattering from O_2.

4.2. Elastic and Momentum-Transfer Cross Sections

A number of papers reported theoretical and experimental values of the differential cross section (DCS) for elastic scattering. Here those DCS are plotted against collision energies and the best values are determined for a set of scattering angles. Use is made of the data obtained by Trajmar *et al.*,[73,74] Linder and Schmidt,[75] Bromberg,[76] Wakiya,[77] Daimon *et al.*,[78] and Shyn and Sharp.[79] From the DCS thus determined, the elastic (Q_{elas}) and momentum-transfer (Q_m) cross sections are calculated. The resulting cross sections are presented in Fig. 4.2. This Q_{elas} has been confirmed to be consistent with Q_T (i.e., $Q_{elas} \leqslant Q_T$) shown in Fig. 4.1 within the errors claimed for them.

There are rather large discrepancies among the DCS reported by the authors mentioned above. Furthermore the data on the DCS are fragmentary and available only for a limited number of energies. Thus it is difficult to determine any reliable recommended values of Q_{elas} and Q_m. The result shown in Fig. 4.2 has an uncertainty of $\sim 20\%$ for the energy range 1–100 eV and $\sim 10\%$ otherwise.

Finally it should be noted that the elastic cross section here includes the effect of rotational transition (see the discussion in Itikawa *et al.*[1]) More strictly the present Q_{elas} is for the vibrationally elastic process.

5. Electron Collisions: Rotational Transitions

No beam experiment has been done so far to determine the cross section for any rotational transition in $e + O_2$ collisions. In their analysis of swarm experiments, Lawton and Phelps[80] assumed the rotational cross section calculated by the Born approximation with an effective quadrupole moment q_{eff} of -0.3 a.u. (1 a.u. $= 1.35 \times 10^{-26}$ esu cm^2). The

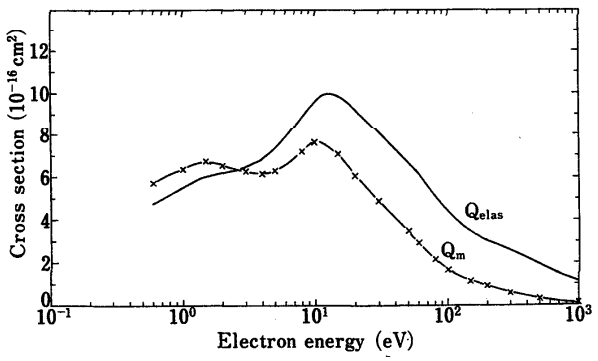

FIG. 4.2. Elastic (Q_{elas}) and momentum-transfer (Q_m) cross sections for electron collisions with O_2.

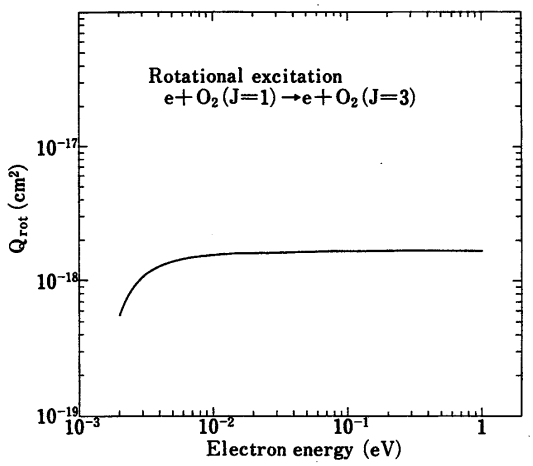

FIG. 5.1. Cross section for the rotational excitation $J = 1 \rightarrow 3$ calculated in the Born approximation, taking account of the interaction between electron and quadrupole moment of O_2.

cross section thus obtained for the rotational transition $J = 1 \rightarrow 3$ is presented in Fig. 5.1. Smith and Dean[81] measured the cooling rate of electrons in O_2 gas over the temperature range 350–800 K. They concluded that their result is well explained by a rotational cross section of the Born type with q_{eff} of -0.5 a.u. The Born cross section is proportional to q_{eff}^2 so that the rotational cross section proposed by Smith and Dean is about three times larger than that shown in Fig. 5.1. At present no definite conclusion can be drawn about the absolute magnitude of the rotational cross section for O_2.

As in the case of vibrational excitation, a resonance scattering through formation of O_2^- can affect the rotational excitation. In fact Lawton and Phelps consider also the resonance contribution to the rotational cross section in the region 0.08–1.65 eV. They are based on the theory of Parlant and Fiquet–Fayard.[82] The latter authors, however, calculated the cross section only for the vibrationally elastic process and gave no details of the rotational structure. The overall feature of the resonance may be similar to the corresponding part of the vibrational cross section shown in Fig. 6.1.

Studies with more credibility are needed for the rotational excitation of oxygen molecules.

6. Electron Collisions: Vibrational Excitations

6.1. $E > 2$ eV

Trajmar *et al.*[73,74] determined the vibrational cross section for electron energies of 4–45 eV from their measurement of electron energy loss spectra of O_2. They reported only the sum

$$Q_{\text{vib}}(\Sigma) = \sum_{v'} Q_{\text{vib}}(0 \rightarrow v') \,. \tag{6.1}$$

The values are shown in Fig. 6.1.

Wong *et al.*[83] measured the differential cross section (DCS) for the vibrational excitations $v = 0 \rightarrow v' = 1,2,3,4$ at a scattering angle of 25° in the energy range 4–15 eV. All the DCS have a broad maximum at ~9.5 eV. (They ascribed this to a shape resonance in which a p wave electron is captured in the field of O_2 $X\,^3\Sigma_g^-$.) The DCS for the excitation $0 \rightarrow 1$ has the value of 4.6×10^{-18} cm^2/sr at the peak. The maximum values for $v' = 2,3,4$ are successively reduced by approximately a factor of 2. On the consideration of this, about one-half of the $Q_{\text{vib}}(\Sigma)$ shown in Fig. 6.1 corresponds to $Q_{\text{vib}}(0 \rightarrow 1)$. If we simply assume an isotropic angular distribution, the DCS measured by Wong *et al.* could be converted into the integral cross section Q_{vib}. From the relative measurement of the angular distribution made by Tronc and Azria,[84] however, the DCS shows a forward peaking. Thus it is difficult to deduce any reliable value of Q_{vib} from the DCS measurement of Wong *et al.*

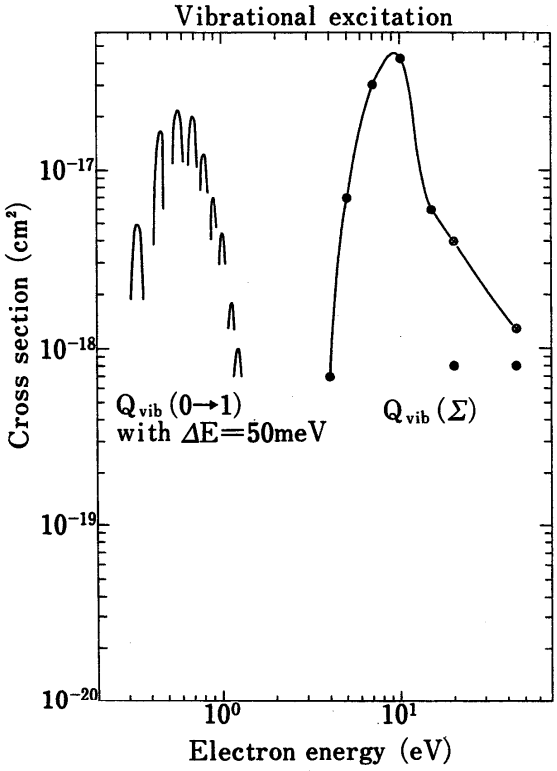

FIG. 6.1. Vibrational excitation cross sections. In the energy region below 2 eV, resonant cross sections (Linder and Schmidt) for $v = 0 \rightarrow 1$ are shown, assuming a resonance width of 50 meV. In the higher energy region, the cross section summed over the final vibrational states. [Trajmar *et al.*, (Refs. 73 and 74)] is presented. The solid line in the region is drawn only for guiding the eyes.

6.2. $E < 2$ eV

Linder and Schmidt[75] observed a very sharp resonance in the vibrational cross section in the region 0.3–1.0 eV. This is interpreted to occur through the temporary capture of the electron to form O_2^- ($^2\Pi_g$). Due to the narrowness of the resonance, Linder and Schmidt give only the cross section multiplied by the resonance width ($Q_{\text{vib}} \cdot \Delta E$). Those values are given in Table 6.1. As an illustration, Fig. 6.1 shows $Q_{\text{vib}}(0 \rightarrow 1)$ derived from the $Q_{\text{vib}} \cdot \Delta E$ in Table 6.1 with the assumption of $\Delta E = 50$ meV. The actual value of ΔE is possibly much smaller than 50 meV (see the theoretical estimate shown in Table 6.1). Then the real cross section at the resonance should be much larger than those shown in Fig. 6.1.

TABLE 6.1. Energy integrated cross section for the vibrational excitation $v = 0 \rightarrow v'$ of O_2 at the resonance due to the temporary capture of electron. The vibrational quantum number of the resonant state (O_2^-) is indicated by v''. Theoretical value of the resonance width is also shown.

E (eV)	$Q_{vib}(0 \rightarrow v') \times \Delta E(10^{-16}$ cm^2 eV)[a] $v'=1$	2	3	4	ΔE(theoretical)[b] (10^{-3} eV)
0.330 ($v''=6$)	0.0025				0.18
0.450 (7)	0.0082				0.33
0.569 (8)	0.0110	0.000 85			0.52
0.686 (9)	0.0100	0.002 5			0.72
0.801(10)	0.0061	0.003 2	0.000 13		0.94
0.914(11)	0.0035	0.002 8	0.000 55		1.2
1.025(12)	0.0017	0.001 9	0.000 73		1.4
1.135(13)	0.0009	0.001 2	0.000 70	0.000 10	1.6
1.242(14)	0.0005	0.000 58	0.000 58	0.000 19	1.8
1.346(15)		0.000 24	0.000 33	0.000 20	2.1
1.449(16)		0.000 11	0.000 18	0.000 17	2.3
1.550(17)			0.000 10	0.000 13	2.5
1.649(18)				0.000 10	2.6

[a] Reference 75.
[b] Reference 82.

On the other hand, the total scattering cross section (Q_T), which should include Q_{vib}, does not show any sharp structure around 1 eV (see Fig. 4.1). The vibrational cross section at the resonance, therefore, is not so large that Q_T is affected. Linder and Schmidt observed similar resonances also in the excitation of higher states ($v' = 2, 3, 4$). The results are given in Table 6.1.

7. Electron Collisions: Electronic Excitations (Including Dissociative Excitations)

7.1. Production of Excited States of the Molecule

7.1.a. $B\,^3\Sigma_u^-$

Trajmar *et al.*[74] and Wakiya[77] measured the cross section for the excitation of O_2 ($B\,^3\Sigma_u^-$). The results are shown in Fig. 7.1. Wakiya claimed the accuracy of his measurement to be 30%–40% at the energies 30–150 eV and 10%–20% otherwise. The experiment of Trajmar *et al.* probably includes more errors than that of Wakiya (see, for example, Trajmar *et al.*[73]). With these uncertainties taken into account, the two sets of data agree well. Since the transition $X\,^3\Sigma_g^- \rightarrow B\,^3\Sigma_u^-$ is optically allowed, the cross section $Q_{exc}(B\,^3\Sigma_u^-)$ should have a Bethe asymptote [$\sim (\ln E)/E$] at higher collision energies. In fact, Wakiya shows that his cross section can be well fitted by the formula

$$Q_{exc}(B\,^3\Sigma_u^-) = [1.24\times10^{-15}\ \text{cm}^2/E(\text{eV})] \times \ln[E(\text{eV})/3.4]\,. \quad (7.1)$$

This is consistent with the Bethe formula with an optical oscillator strength of 0.161 and an excitation threshold of 8.44 eV. This Bethe cross section is also plotted in Fig. 7.1.

Chung and Lin[85] calculated the cross section by using the Born–Ochkur approximation. For comparison, their cross section is shown in Fig. 7.1. The Born approximation is usually less reliable at lower energies. In the present case, the cross section of Chung and Lin, however, may serve as an extrapolation of the cross section to the region near threshold, where no experimental data are available.

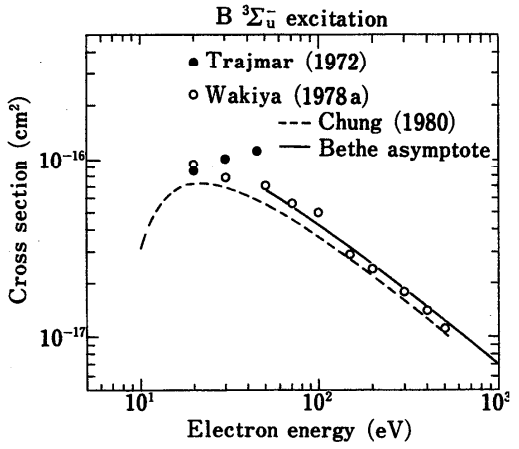

FIG. 7.1. Cross section for excitation of the $B\,^3\Sigma_u^-$ state, measured by Trajmar *et al.*, (Ref. 85), (●) and Wakiya (Ref. 77) (○) and calculated by Chung and Lin (---). The Bethe asymptote [Eq. (7.1)] is also given (—).

7.1.b. $a\,^1\Delta_g$ and $b\,^1\Sigma_g^+$

For these lower lying excited states of O_2, there are three independent measurements of the excitation cross section (Linder and Schmidt[75]; Trajmar *et al.*[73,74]; Wakiya[86]). They are shown in Figs. 7.2 and 7.3 and are in good agreement with each other. Recently Noble and Burke[87] made an elaborate calculation of the cross section using the R-matrix method. Their result is compared with the experimental data in Figs. 7.2 and 7.3. The agreement between theory and experiment is very good. From these comparisons, we can conclude that the cross section for the excitation of these states is

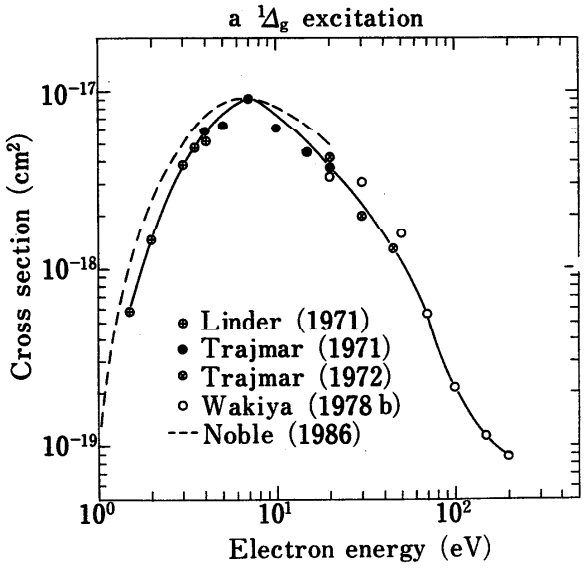

FIG. 7.2. Cross section for excitation of the $a\,^1\Delta_g$ state, measured by Linder and Schmidt, (Ref. 75) Trajmar *et al.* (Refs. 73 and 74) and Wakiya (Ref. 86). A solid line is drawn smoothly through the experimental data points. Theoretical values obtained by Noble and Burke (Ref. 87) are shown for comparison.

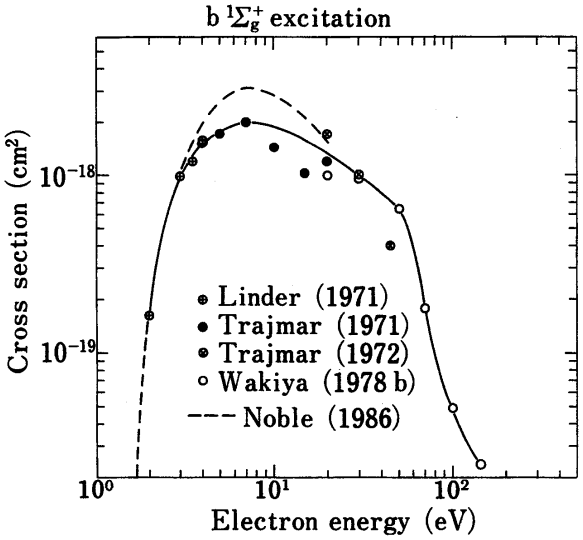

FIG. 7.3. The same as Fig. 7.2, but for the excitation of $b\ ^1\Sigma_g^+$ state.

known with a fair amount of confidence. Teillet-Billy *et al.*[88] have shown theoretically that the excitation of these states occurs mostly through the $O_2^-(^2\Pi_g)$ shape resonance.

7.1.c. Other Excited States

The three states, $A\ ^3\Sigma_u^+, C\ ^3\Delta_u$ and $c\ ^1\Sigma_u^-$, are too closely located to be resolved experimentally. The excitation cross section of the sum of these three states was measured by Trajmar *et al.*[74] and Wakiya[86]. Those are given in Fig. 7.4. The two groups obtained also the excitation cross section for the collection of states in the 9.7–12.1 eV region. These cross sections are presented in Fig. 7.5. Wakiya[86] suggested that the dominant contribution to this cross section comes from the optically allowed excitation of the state $E\ ^3\Sigma_u^-$.

The cross sections mentioned above were measured

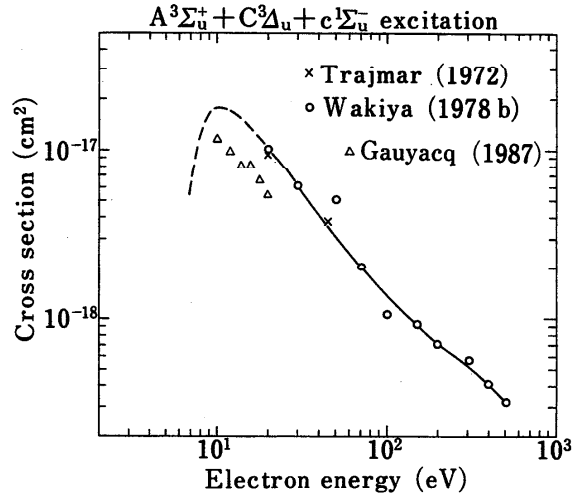

FIG. 7.4. Cross section for excitation of the sum of states $A\ ^3\Sigma_u^+, C\ ^3\Delta_u$ and $c\ ^1\Sigma_u^-$, measured by Trajmar *et al.* (Ref. 74) and Wakiya (Ref. 86). The solid line is drawn through the experimental data and the dashed line is its extrapolation to the lower energy region. Preliminary data of a recent measurement (Ref. 89) are also shown for comparison.

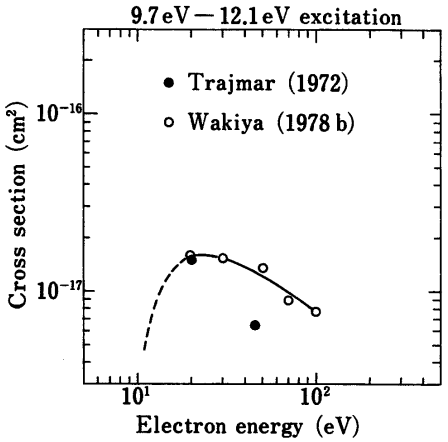

FIG. 7.5. The same as Fig. 7.4, but for excitation of the sum of states with excitation energies between 9.7 and 12.1 eV.

only for energies higher than 20 eV. Hayashi (unpublished) attempted to extrapolate them to the lower-energy region. He made the extrapolation so as to be compatible with the swarm analysis of oxygen discharge. His result is shown in Figs. 7.4 and 7.5. Very recently Gauyacq *et al.*[89] reported their measurement of the cross section Q_{exc} $(A + C + c)$ at the lower energies. Their data are also shown in Fig. 7.4. If account is taken of the crudeness of the extrapolation and the large experimental error ($\pm$ 50%), the two results are not much different.

7.2. Dissociative Excitation

7.2.a. Total Cross Section for Dissociation

No reliable data are available for the total cross section for dissociation of oxygen molecules. For the excited states $A\ ^3\Sigma_u^+, C\ ^3\Delta_u, c\ ^1\Sigma_u^-$, and $B\ ^3\Sigma_u^-$, only the repulsive portion of the potential curve lies in the Franck–Condon region of the ground state. Thus an excitation of any of these states results mostly in dissociation of O_2. We can, therefore, simply assume

$$Q_{diss} = Q_{exc}(B\ ^3\Sigma_u^-) + Q_{exc}(A\ ^3\Sigma_u^+ + C\ ^3\Delta_u + c\ ^1\Sigma_u^-). \quad (7.2)$$

The cross sections on the right-hand side of the equation are shown in the previous subsection (Figs. 7.1 and 7.4).

With the use of this estimate of Q_{diss}, Eliasson and Kogelschatz[90] evaluated the yield of O_3 produced in an oxygen discharge. With this method they succeeded in explaining their experimental result within an error of 30%.

7.2.b. Production of Excited Oxygen Atoms (Emission Cross Sections)

Many papers have been published on the measurement of emission from the dissociation fragment O. In particular, an extensive study was made by Ajello and Franklin[91] and Schulman *et al.*[92] for the emission of VUV and visible-IR light, respectively. Both groups made detailed comparisons of their own measurement with others. Usually the emission cross section has its maximum in the collision energy region 100–200 eV. Table 7.1 lists the processes for which the maximum cross section is known to exceed 10^{-18} cm^2. Cross sec-

TABLE 7.1. Emission from oxygen atoms at the electron-impact dissociation of O_2. The lines for which the maximum of the emission cross section (Q_{emis}) exceeds 10^{-18} cm^2 are listed.

Wavelength (nm)	Transitions	Q_{emis} (at 100 eV)[b] (10^{-18} cm^2)	References
98.9	$3s'\,^3D$–$2p^4\,^3P$	1.3 [c]	f
130.4	$3s\,^3S$–$2p^4\,^3P$	3.16[d]	g
(135.6	$3s\,^5S$–$2p^4\,^3P$	6.9	h)[a]
777.4	$3p\,^5P$–$3s\,^5S$	4.30	i
844.7	$3p\,^3P$–$3s\,^3S$	2.00[e]	i
926.6	$3d'\,^5D$–$3p^4\,^5P$	1.24	i

[a] Preliminary result.
[b] Typical examples of the data.
[c] More data shown in Fig. 7.7.
[d] More data are shown in Fig. 7.6.
[e] More data are shown in Fig. 7.8.
[f] Reference 91.
[g] Reference 93.
[h] Reference 95.
[i] Reference 92.

tions for many other processes are reported by Ajello and Franklin and Schulman *et al.* (and the papers cited by them), but most of them are given only at one point of energy. Cross sections for some sample processes are shown below.

Figure 7.6 shows the cross section for emission of 130.4 nm from the transition $2p^3 3s\,^3S^0 \rightarrow 2p^4\,^3P$ of oxygen atoms; four different sets of the cross section are compared. The methods utilized to normalize the cross section vary. Zipf[93] employed as standard the cross section recently remeasured for Ly-α emission of H resulting from collisions of e and H_2 (7.5×10^{-18} cm^2 $\pm$ 10% at 100 eV, Risley, private communication). Aarts and de Heer[113] used the emission cross section for the transition $A\,^1\Pi \rightarrow X\,^1\Sigma^+$ of CO. Lawrence[24] obtained the absolute value of Q_{emis} by using the cascading relation between the emissions of 130.4 and 844.7 nm radiations from the oxygen atom. Ajello[94] also normalized his data to the $A\,^1\Pi \rightarrow X\,^1\Sigma^+$ emission of CO. Recently, however, Ajello and Franklin remeasured the cross section, normalizing to the Ly-α emission cross section newly determined by themselves [$(8.2 \pm 1.2)\times10^{-18}$ cm^2 at 100 eV]. They reported their result only for the electron energy of 200 eV. In Fig. 7.6, Ajello's old data are plotted but renormalized to the new measurement of Ajello and Franklin at 200 eV. When we take into account the difficulty in getting reliable cross sections from such emission measurements, the agreement of the four results in Fig. 7.6 is remarkably good.

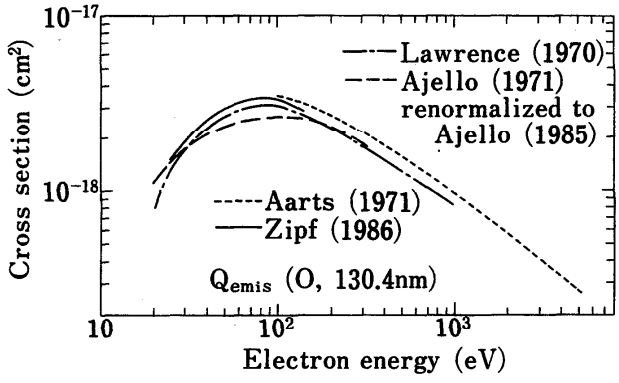

FIG. 7.6. Emission cross section for the 130.4-nm line of O upon electron impact dissociation of O_2. Four sets of experimental data are shown: Lawrence[124], Ajello (Ref. 94) renormalized to the measurement by Ajello and Franklin, (Ref. 91) Aarts and de Heer, (Ref. 113) and Zipf (Ref. 93).

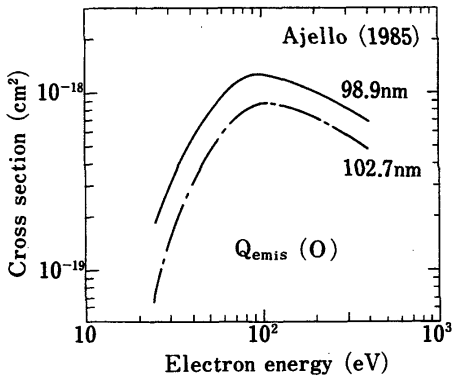

FIG. 7.7. Emission cross section for the 98.9- and 102.7-nm lines of O upon electron impact dissociation of O_2.[91]

Figure 7.7 gives two sets of cross sections which have a large value for the VUV emission. Those emissions are from $2p^3 3s'\,^3D^0$–$2p^4\,^3P$ (98.9 nm) and $2p^3 3d\,^3D^0$–$2p^4\,^3P$ (102.7 nm) and measured by Ajello and Franklin. As an example of the IR emission, Fig. 7.8 presents two sets of cross sections (Lawrence; Schulman *et al.*) for the emission $2p^3 3p\,^3P$–$2p^3 3s\,^3S^0$ (844.7 nm).

Ajello[94] measured also the emission of 135.6 nm from the transition $2p^3 3s\,^5S^0 \rightarrow 2p^4\,^3P$. In this case the fragment atom has a long life against radiative decay. It is, therefore, difficult to collect all the emission during the stay of the atom in the collision volume. Ajello thus gave the lower limit of the emission cross section for the process to be 1.65×10^{-18} cm^2 at 100 eV. Zipf[95] presented, in his review article, a preliminary result of the measurement of this emission cross section: 6.9×10^{-18} cm^2 at 100 eV. No details of the measurement have yet been published.

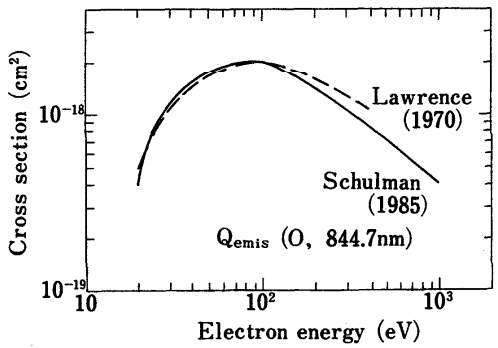

FIG. 7.8. Emission cross section for the 844.7-nm line of O upon electron impact dissociation of O_2. Two sets of experimental data are shown: Schulman *et al.* (Ref. 92) and Lawrence (Ref. 124).

8. Electron Collisions: Attachment

When an electron collides with O_2, a negative ion is produced through the following two mechanisms:

(1) dissociative attachment

$$e + O_2 \rightarrow O^- + O\,, \tag{8.1}$$

(2) nondissociative attachment

$$e + O_2 \rightarrow O_2^{-*} \underset{+M}{\rightarrow} O_2^-\,. \tag{8.2}$$

A third process is possible:

(3) radiative attachment

$$e + O_2 \rightarrow O_2^- + h\nu\,. \tag{8.3}$$

The probability of Eq. (8.3), however, is extremely small. There is no direct measurement of the cross section for Eq. (8.3) reported so far. Using the detailed balancing relation, the cross section for Eq (8.3) was estimated from the cross section for the photodetachment of O_2^- (Branscomb[96]). That gives cross section values 1.3×10^{-24}, 6.1×10^{-24}, and 1.5×10^{-23} cm^2 at collision energies 1, 2, and 3 eV, respectively. These values, however, should be regarded as crude estimates, because no account has been taken of the rotational–vibrational structure of O_2 and O_2^-. In the following, only the processes Eqs. (8.1) and (8.2) are discussed in detail.

8.1. Dissociative Attachment

This process has been investigated by many people and general agreement on the cross section has been reached (see, for example, a review by Christophorou[97]). As a typical example, Fig. 8.1 shows the value measured by Schulz.[98] The cross section has a broad peak with its maximum at about 6.7 eV. This peak is interpreted as a resonance process

$$e + O_2(X\,^3\Sigma_g^-) \rightarrow O_2^-(^2\Pi_u) \rightarrow O^-(^2P) + O(^3P)\,. \tag{8.4}$$

For collision energies above 17 eV, O^- can be produced through the process of ion pair formation

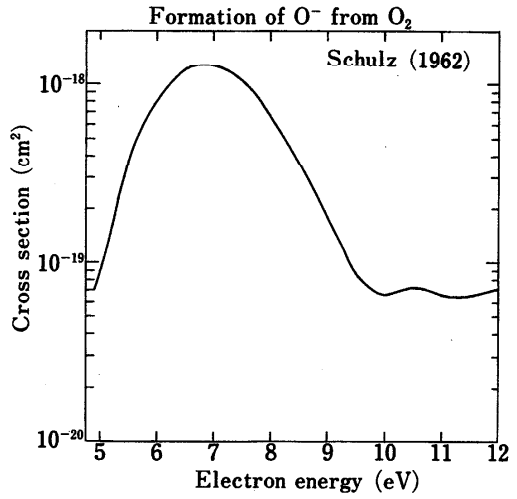

FIG. 8.1. Cross section for the production of O^- at the electron collision with O_2.[98]

$$e + O_2 \rightarrow O^+ + O^- + e\,. \tag{8.5}$$

Rapp and Briglia[99] measured O^- over the energy range of 4–55 eV. They found that, after the broad peak shown in Fig. 8.1, the yield of O^- increases above 17 eV. They suggested that the increase is due to the process (8.5). According to the measurement, the cross section for Eq. (8.5) is almost constant above 25 eV and has a value of 0.35×10^{-18} cm^2.

8.2. Nondissociative Attachment

The process (8.2) has been experimentally studied with an electron beam, or swarm technique. From those experimental studies, together with theoretical ones, the attachment process for thermal electrons is understood to proceed in the following way (see, for example, a review by Hatano[100]). First the electron of $\sim$80 meV is resonantly captured by O_2:

$$e + O_2(X\,^3\Sigma_g^-, v=0) \rightarrow O_2^{-*}(^2\Pi_g, v'=4)\,. \tag{A}$$

The lifetime of the resonant state (O_2 *) in terms of the autodetachment of electrons:

$$O_2^{-*}(^2\Pi_g, v'=4) \rightarrow O_2(X\,^3\Sigma_g^-, v=0) + e \tag{B}$$

is known to be $\sim$100 ps, which gives a resonance width of $\sim 10\,\mu$eV. In a gas, de-excitation of O_2^{-*} can occur by collision with a third body M. That is, the decaying process (B) competes with

$$O_2^{-*}(^2\Pi_g, v'=4) + M \rightarrow O_2^-(^2\Pi_g, v' \leqslant 3) + M\,. \tag{C}$$

The latter process results in a stable negative ion of the oxygen molecule.

When electrons are introduced into oxygen gas, they are thermalized and ultimately attached to the oxygen molecules. The effective (two-body) rate constant, k_{eff}, for attachment was found to be proportional to the pressure of oxygen [O_2], unless that is too high:

$$k_{\text{eff}} = k_{O_2}[O_2]\,. \tag{8.6}$$

The quantity k_{O_2} is the overall three-body rate constant for the process

$$e + O_2 + O_2 \rightarrow O_2^- + O_2$$

and has been measured by many people. Their results are in general agreement (Hatano[100]). The typical value, which was obtained by Shimamori and Fessenden,[101] is

$$k_{O_2} = (2.26 \pm 0.10)\times10^{-30}\ \text{cm}^6/\text{s} \quad \text{at 298 K.}$$

We can regard this attachment process as caused by steps (A), (B), and (C), described above, with the oxygen molecule as the third body in (C) (i.e., M = O_2). Then the effective rate constant is given by

$$k_{\text{eff}} = (k_A k_C[O_2])/(k_B + k_C[O_2])\,, \tag{8.7}$$

where k_A, k_B, and k_C are the rate constants for the processes (A), (B), and (C), respectively. When [O_2] is small, Eq. (8.7) is reduced to the form of Eq. (8.6) and the coefficient k_{O_2} is given by

$$k_{O_2} = k_A k_C / k_B\,. \tag{8.8}$$

From the experimental study of mixtures of oxygen with various molecules Toriumi and Hatano,[102] using a rela-

tion like Eq. (8.7), determined the value of k_A to be 3×10^{-11} cm^3/s.

Recently the electron attachment to O_2 van der Waals molecules such as O_4 and $O_2\cdot M$ has been observed (Hatano and Shimamori[103]; Hatano[100]). The effect of the van der Waals interaction between O_2 and O_2 or M on the attachment resonance has been discussed in detail. The values of k_{eff} have been measured by systematically varying the temperature and pressure of gases. Up to a pressure of 10 Torr, the relation (8.6) holds. The temperature dependence of the three-body rate constant, k_{O_2}, is shown in Fig. 8.2 (Shimamori and Fessenden). The experimental results at lower temperatures deviate strongly from the result (the dashed line) estimated from the mechanism mentioned above. Instead, the experimental result is well explained by another mechanism: a dissociative attachment to a dimer, e.g., O_4. The dimer is formed through

$$O_2 + O_2 \rightleftarrows O_4 . \qquad (D)$$

An electron attachment occurs as

$$e + O_4 \rightleftarrows O_4^{-}{}^{*} \rightarrow O_2^{-} + O_2 . \qquad (E)$$

The processes (D) and (E) combined also result in k_{eff} being linearly proportional to $[O_2]$. The kinetic analysis of measured values of k_{eff} based on this mechanism gives an estimate of the rate constant for electron attachment to O_4 of $\sim10^{-9}$ cm^3/s, which is much larger than k_A. This large enhancement of the attachment rate constant has been explained in terms of a decrease in the attachment resonance energy due to the van der Waals interaction. This has been

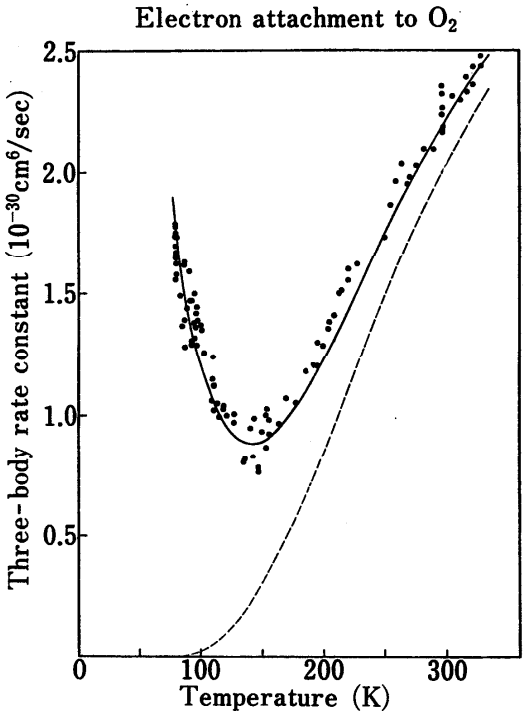

FIG. 8.2. Temperature dependence of the three body rate constant for electron attachment to O_2.[101] Black circles are measured values. Lines show the rate constant calculated in resonance theory with (—) and without (---) including the effect of attachment to van der Waals molecules.

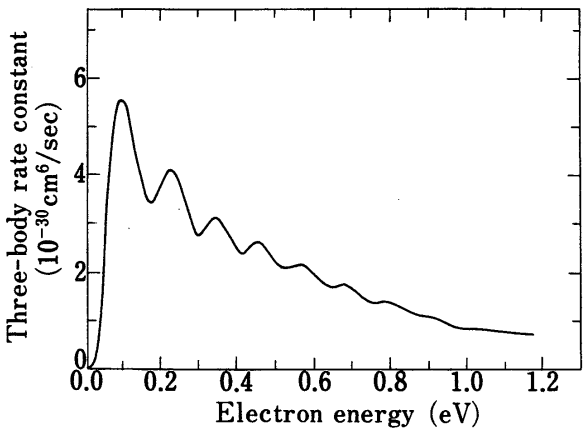

FIG. 8.3. The electron-energy dependence of the three body rate constant for electron attachment to O_2 (Ref. 106).

recently confirmed by beam experiments (Märk *et al.*[104]; Stamatovic[105]).

Finally, brief mention is made of the dependence of the rate constant on electron energy. Spence and Schulz[106] injected a beam of electrons with an energy spread of 80–100 meV into oxygen gas. They detected O_2^-, whose yield was found proportional to the pressure squared. They determined the absolute magnitude of the O_2^- yield, normalized to that of O^-. Figure 8.3 shows the measured values of the effective rate constant, i.e., the three-body attachment cross section multiplied by the beam velocity. Peaking structure due to the resonance capture is apparent. Each peak corresponds to the vibrational level of the captured state (O_2^-). The first peak at about 0.09 eV arises from the process (A). The rate constant averaged over the velocity distribution of electrons should give the k_{O_2} shown in Fig. 8.2.

9. Electron Collisions: Ionization (Including Dissociative Ionization)

9.1. Cross Sections for Ion Production

9.1.a. Gross Ionization Cross Section

From ion current measurement, the gross (or total) ionization cross section is derived. It is defined by

$$Q_{ion}(\text{gross}) = \sum_m m Q_{ion}(O_2^{m+}) + \sum_n n Q_{ion}(O^{n+}) , \qquad (9.1)$$

where $Q_{ion}(O_2^{m+})$ is the ionization cross section for the production of O_2^{m+} and $Q_{ion}(O^{n+})$ that for the dissociative ionization producing O^{n+}. The most reliable data for Q_{ion} (gross) are those obtained by Rapp and Englander-Golden[107] (see the review by de Heer and Inokuti[108]). Their values are plotted in Fig. 9.1. The accuracy is within $\sim10\%$. One should note that the method of correction for the McLeod gauge used for the pressure measurement is somewhat different for O_2 than for other molecules. This might affect the reliability of the resulting cross section for O_2.

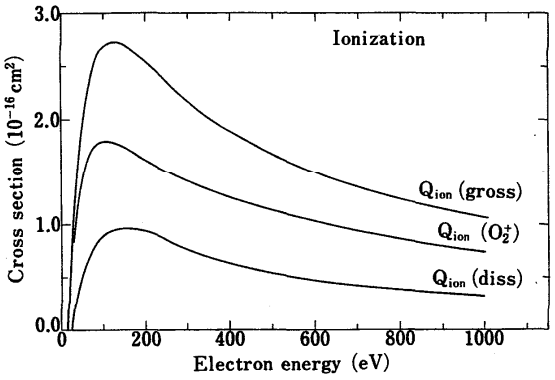

FIG. 9.1. Cross sections for electron-impact ionization of O_2. Q_{ion} (gross): gross ionization cross section; Q_{ion} (O_2^+): cross section for production of O_2^+; Q_{ion} (diss): dissociative ionization cross section.

9.1.b. Production of O_2^+ and O_2^{2+}

Märk[109] reported the cross sections $Q_{ion}(O_2^+)$ and $Q_{ion}(O_2^{2+})$ for electron energies < 166 eV. The method of measurement is identical to that for N_2. In the case of N_2, it has been suggested that a rather large systematic error is involved in the determination of the absolute value of the cross section (Itikawa *et al.*[1]). Instead of using Märk's values, therefore, we take the same procedure of determining Q_{ion} for O_2 as for N_2. That is, $Q_{ion}(O_2^+)$ is derived from the relation

$$Q_{ion}(O_2^+) = Q_{ion}(\text{gross}) - Q_{ion}(\text{diss}) , \qquad (9.2)$$

where Q_{ion} (diss) is the dissociative ionization cross section determined in the next subsection. The resulting $Q_{ion}(O_2^+)$ is shown in Fig. 9.1 and compared in Fig. 9.2 to the cross section obtained by Märk. Märk's value is smaller than the present one by as much as 32%.

According to Märk, the ratio $Q_{ion}(O_2^{2+})/Q_{ion}(O_2^+)$ is $< 1\%$ throughout the electron-energy range considered (< 166 eV). In relation (9.2), therefore, the contribution of O_2^{2+} has been ignored.

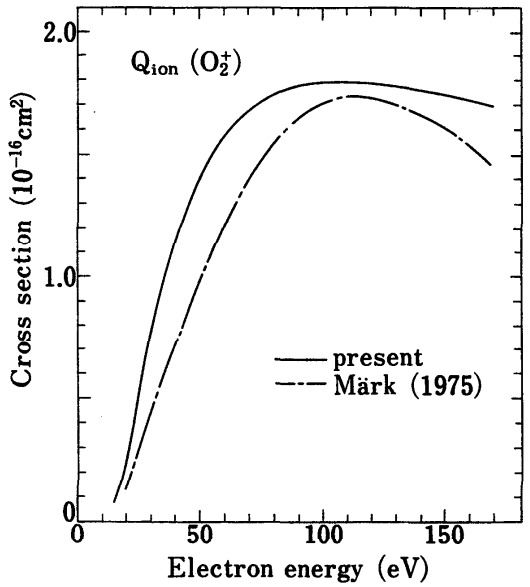

FIG. 9.2. Cross section for production of O_2^+. The present values are compared with those measured by Märk (Ref. 109).

9.1.c. Dissociative Ionization

Rapp *et al.*[110] measured the dissociative ionization cross section

$$Q_{ion}(\text{diss}) = \sum_n n Q_{ion}(O^{n+}) . \qquad (9.3)$$

Their values have to be corrected in consideration of the following two factors: They detected only the fragment ions with kinetic energy larger than 0.25 eV and they used the McLeod gauge for the pressure measurement. No quantitative estimate of the correction factor is available for oxygen. Here we assume the same correction factor as in the case of nitrogen (Itikawa *et al.*). Then we obtain Q_{ion} (diss) shown in Fig. 9.1. The above assumption about the correcting procedure may not be valid. The amount of the resulting correction is so small that the ambiguity of the correction procedure introduces little, if any, significant error.

9.2. Production of Excited Ions from O_2

9.2.a. Excited States of O_2^+

Several papers reported the measurement of emission from O_2^+ produced by electron impact on O_2. Fig. 9.3 shows the emission cross section for the (1,0) band of the first negative system, $b\,^4\Sigma_g^- \rightarrow a\,^4\Pi_u$ of O_2^+. The cross section obtained by Borst and Zipf[111] is shown in Fig. 9.3 as a typical example. For a higher energy, the result of the measurement by Aarts and de Heer (cited in McConkey and Woolsey[114]) is plotted. Their original values are in a relative scale. In Fig. 9.3, their data have been normalized to the cross section of Borst and Zipf at 100 eV. There are several other measurements for this system and, considering the difficulty of these measurements, they agree well with the values shown in Fig. 9.3.

If we ignore cascade effects and employ the Franck–Condon factor approximation for the excitation of associated vibrational levels, we can derive the excitation cross section Q_{exc} from the corresponding emission one Q_{emis} (see,

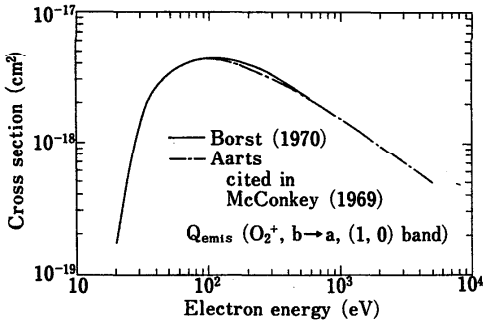

FIG. 9.3. Emission cross section for the (1,0) band of the first negative system, $b\,^4\Sigma_g^- \rightarrow a\,^4\Pi_u$ of O_2^+, measured at the electron collision with O_2 by Borst and Zipf (Ref. 111) and Aarts and de Heer. The latter are cited on McConkey and Woolsey (Ref. 114) and normalized to the value of Borst and Zipf at 100 eV.

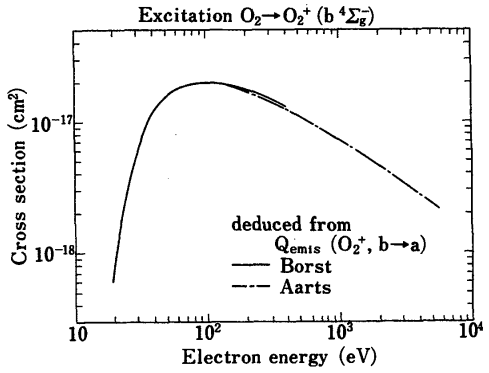

FIG. 9.4. Cross section for production of O_2^+ in its $b\,^4\Sigma_g^-$ state by collision of electrons with O_2. The values derived from the emission cross section in Fig. 9.3 are shown.

for example, Aarts and de Heer[112]). In this way, Q_{exc} for O_2 $(X\,^3\Sigma_g^-) \rightarrow O_2^+ (b\,^4\Sigma_g^-)$ has been determined from the Q_{emis} in Fig. 9.3 and is shown in Fig. 9.4. In this and the following cases, use is made of the Franck–Condon factors compiled by Krupenie.

Stewart and Gabathuler[126] and McConkey and Woolsey measured the Q_{emis} for the second negative system $A\,^2\Pi_u$-$X\,^2\Pi_g$ of O_2^+. They made the measurements only at the electron energy of 100 eV. The values are of the order of 10^{-20} cm^2 and much smaller (by $\sim 10^{-2}$) than the cross section for the first negative system (see Fig. 9.3). From this Q_{emis} for the second negative system, we can deduce the excitation cross section for $O_2(X\,^3\Sigma_g^-) \rightarrow O_2^+ (A\,^2\Pi_u)$ to be $\sim 3\times 10^{-17}$ cm^2 at 100 eV. This value, however, is accompanied by a large uncertainty, because the experimental evidence shows a breakdown of the Franck–Condon factor approximation in this case.

9.2.b. Excited States of O^+

Ajello and Franklin[91] measured UV emissons from O^+ induced by electron impact with O_2. They reported several emission processes, but only the transition $2s2p^4\,^4P \rightarrow 2s^22p^3\,^4S^0$ (83.3 nm) has a cross section exceeding 10^{-18} cm^2, illustrated in Fig. 9.5. For comparison, the cross section obtained by Aarts and de Heer[113] for the same process is also shown. The two sets of data are in agreement within the combined errors (22% for Ajello and Franklin and 50% for Aarts and de Heer).

9.3. Energy Distributions of Secondary Electrons

Figure 9.6 gives the energy distributions of secondary (ejected and scattered) electrons upon the electron-impact ionization of O_2. The data shown are based on the measurement by Opal *et al.*[125] Their measurement was restricted to secondary electrons with energies higher than 4 eV. For electrons with lower energies, they proposed to use an empirical function

$$\frac{dQ_{ion}}{dE_s} = \frac{C}{E_s^2 + (15.2)^2} \tag{9.4}$$

for the differential cross section over the secondary electron energy E_s (in eV). Here C is a constant depending on the energy of the incident electron. When they integrate the energy distribution of the secondary electrons shown in Fig. 9.6, together with the empirical function Eq. (9.4), they obtain a total ionization cross section in good agreement with the Q_{ion} (gross) in Fig. 9.1.

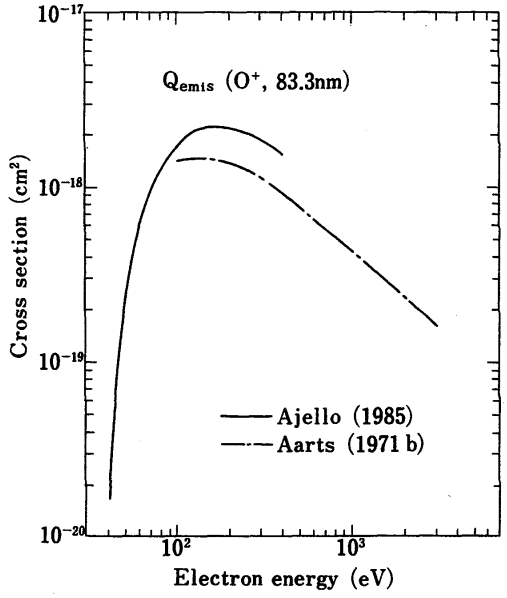

FIG. 9.5. Emission cross section for the 83.3-nm line of O^+ at the electron collision with O_2. Two sets of experimental results are shown: Ajello and Franklin[91] and Aarts and de Heer[113]

10. Summary and Future Problems

Cross sections for electron collisions with oxygen molecules are summarized in Fig. 10.1. Data sources are: the total

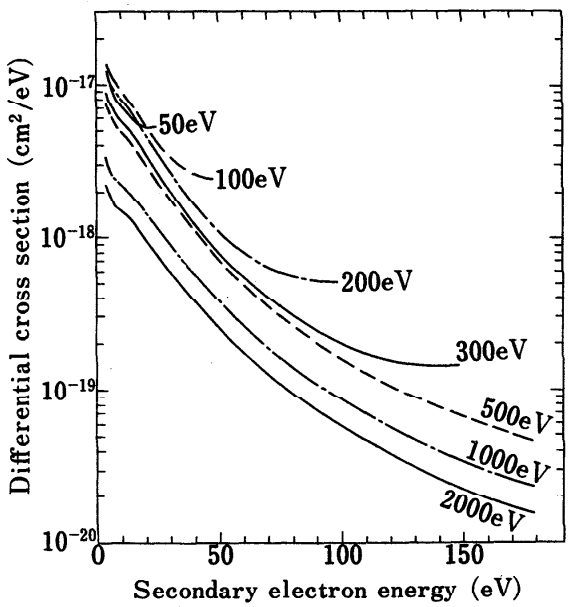

FIG. 9.6. Energy distribution of secondary electrons at the ionizing collision of electrons with O_2. Energy of the incident electron is indicated (Ref. 125).

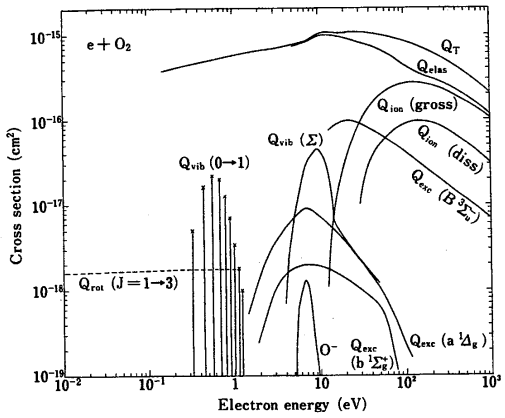

FIG. 10.1. Summary of cross sections for electron collisions with O_2. Representative data are reproduced from figures in the previous sections. Only a schematic presentation is made for the vibrational cross section in the resonance region below 2 eV.

scattering cross section (Q_T) from Fig. 4.1, the elastic cross section (Q_{elas}) from Fig. 4.2, the cross section for the rotational excitation $J=1\rightarrow3$ [Q_{rot} ($J=1\rightarrow3$)] from Fig. 5.1, the cross section for the vibrational excitation from Fig. 6.1, a few representative cross sections for electronic excitations from Figs. 7.1–7.3, the cross section for the dissociative attachment from Fig. 8.1, and the gross and dissociative ionization cross sections from Fig. 9.1.

Collisions of photons and electrons with oxygen molecules are much less studied than those for nitrogen molecules. The oxygen molecule easily dissociates. It can capture an electron to become a negative ion. Its ground state has a triplet spin. Furthermore the perturbations among the electronically excited states of oxygen are very complicated. These properties of the oxygen molecule make its study difficult both theoretically and experimentally. The present paper provides state of the art knowledge of the collision processes involving oxygen molecules and electrons/photons. Much work remains to be done. Future problems are, for instance:

(a) More definitive information is needed on the electron-impact excitation of rotational states of O_2. No quantitative estimate of the resonance effect exists. A beam-type measurement or an elaborate calculation would be necessary.

(b) The resonance structure of the vibrational cross section ~0.3–1.3 eV should be studied in more detail. Rotational motion of the molecule may affect the resonance.

(c) No direct measurement has been done so far on the total cross section for the electron-impact dissociation. Knowledge about fractional yields of dissociation fragments, particularly $O(^3P)$, $O(^1D)$, and $O(^1S)$, is very important.

(d) Cross sections for the excitation of electronic states are still fragmentary. In particular more detailed studies are necessary for highly excited states.

(e) As was mentioned in Sec. 4.2, the agreement among different measurements of the elastic differential cross section is not satisfactory. Further experiments over a wide range of energy and scattering angle would be desirable.

11. Acknowledgments

During the course of this data compilation, many colleagues provided us with valuable information about the data presented here. Particular thanks are due to Dr. R. H. Huebner, who sent us detailed numerical values of his photoabsorption cross section. Thanks are also due to Dr. J. P. Gauyacq for providing us with the details of the study of electronic excitation of O_2.

12. References

[1]Y. Itikawa, M. Hayashi, A. Ichimura, K. Onda, K. Sakimoto, K. Takayanagi, M. Nakamura, H. Nishimura, and T. Takayanagi, J. Phys. Chem. Ref. Data **15**, 985 (1986).
[2]A. V. Phelps, in *Swarm Studies and Inelastic Electron-Molecule Collisions*, edited by L. C. Pitchford, B. V. McKoy, A. Chutjian, and S. Trajmar (Springer, New York, 1987), p. 127.
[3]P. H. Krupenie, J. Phys. Chem. Ref. Data **1**, 423 (1972).
[4]K. P. Huber and G. Herzberg, *Molecular Spectra and Molecular Structure IV* (Van Nostrand, New York, 1979).
[5]J. H. Agee, J. B. Wilcox, L. E. Abbey, and T. F. Moran, Chem. Phys. **61**, 171 (1981).
[6]N. H. F. Beebe, E. W. Thulstrup, and A. Andersen, J. Chem. Phys. **64**, 2080 (1976).
[7]R. P. Saxon and B. Liu, J. Chem. Phys. **67**, 5432 (1977).
[8]R. P. Saxon and B. Liu, J. Chem. Phys. **73**, 870 (1980).
[9]H. H. Michels, in *The Excited State in Chemical Physics, Part 2*, edited by J. W. McGowan (Wiley, New York, 1981), p. 225.
[10]A. A. Christodoulides, D. L. McCorkle, and L. G. Christophorou, in *Electron-Molecule Interactions and their Applications*, edited by L. G. Christophorou (Academic, New York, 1984), Vol. 2, p. 423.
[11]R. J. Celotta, R. A. Bennett, J. L. Hall, M. W. Siegel, and J. Levine, Phys. Rev. A **6**, 631 (1972).
[12]G. Das, A. C. Wahl, W. T. Zemke, and W. C. Stwalley, J. Chem. Phys. **68**, 4252 (1978).
[13]G. Birnbaum and E. R. Cohen, Mol. Phys. **32**, 161 (1976).
[14]G. D. Zeiss and W. J. Meath, Mol. Phys. **33**, 1155 (1977).
[15]M. A. Buldakov, I. I. Matrosov, and T. N. Popova, Opt. Spectrosc. **46**, 488 (1979).
[16]M. A. Buldakov, B. V. Korolev, I. I. Matrosov, and T. N. Popova, Opt. Spectrosc. **62**, 452 (1987).
[17]K. Yoshino, D. E. Freeman, J. R. Esmond, and W. H. Parkinson, Planet. Space Sci. **31**, 339 (1983).
[18]A. S.-C. Cheung, K. Yoshino, W. H. Parkinson, D. E. Freeman, Can. J. Phys. **62**, 1752 (1984).
[19]B. R. Lewis, L. Berzins, and J. H. Carver, J. Quant. Spectrosc. Radiat. Transfer, **36**, 209 (1986).
[20]K. Yoshino, D. E. Freeman, J. R. Esmond, and W. H. Parkinson, Planet. Space Sci. **35**, 1067 (1987).
[21]B. R. Lewis, L. Berzins, J. H. Carver, and S. T. Gibson, J. Quant. Spectrosc. Radiat. Transfer **36**, 187 (1986).
[22]M. Jeunehomme, J. Chem. Phys. **44**, 4253 (1966).
[23]E. H. Fink and K. H. Welge, Z. Naturforsch Teil A **23**, 358 (1968).
[24]R. W. Wetmore, J. L. Fox, and A. Dalgarno, Planet. Space Sci. **32**, 1111 (1984).
[25]J. T. Moseley, P. C. Cosby, J.-B. Ozenne, and J. Durup, J. Chem. Phys. **70**, 1474 (1979).
[26]J. C. Hansen, J. T. Moseley, A. L. Roche, and P. C. Cosby, J. Chem. Phys. **77**, 1206 (1982).
[27]J. H. Black and P. L. Smith, Astrophys. J. **277**, 562 (1984).
[28]R. T. Boreiko, T. L. Smithson, T. A. Clark, and H. Wieser, J. Quant. Spectrosc. Radiat. Transfer **32**, 109 (1984).
[29]J. Berkowitz, *Photoabsorption, Photoionization, and Photoelectron Spectroscopy* (Academic, New York, 1979).
[30]K. Kirby, E. R. Constantinides, S. Babeu, M. Oppenheimer, and G. A. Victor, At. Data Nucl. Data Tables **23**, 63 (1979).
[31]B. E. Cole and R. N. Dexter, J. Phys. B **11**, 1011 (1978).
[32]G. Mehlman, D. L. Ederer, and E. B. Saloman, J. Chem. Phys. **68**, 1862 (1978).
[33]C. E. Brion, K. H. Tan, M. J. van der Wiel, and Ph.E. van der Leeuw, J. Electron Spectrosc. **17**, 101 (1979).

[34]J. A. R. Samson, G. H. Rayborn, and P. N. Pareek, J. Chem. Phys. **76**, 393 (1982).
[35]F. M. Matsunaga and K. Watanabe, Sci. Light **16**, 31 (1967).
[36]P. M. Dehmer and W. A. Chupka, J. Chem. Phys. **62**, 4525 (1975).
[37]R. E. LaVilla, J. Chem. Phys. **63**, 2733 (1975).
[38]D. M. Barrus, R. L. Blake, A. J. Burek, K. C. Chambers, and A. L. Pregenzer, Phys. Rev. A **20**, 1045 (1979).
[39]S. Bodeur, J. Appl. Phys. **47**, 4911 (1976).
[40]J. A. R. Samson, J. L. Gardner, and G. N. Haddad, J. Electron Spectrosc. **12**, 281 (1977).
[41]T. Gustafsson, Chem. Phys. Lett. **75**, 505 (1980).
[42]L. C. Lee, R. W. Carlson, D. L. Judge, and M. Ogawa, J. Quant. Spectrosc. Radiat. Transfer **13**, 1023 (1973).
[43]O. Edqvist, E. Lindholm, L. E. Selin, and L. Asbrink, Phys. Scr. **1**, 25 (1970).
[44]P. Morin, I. Nenner, M. Y. Adam, M. J. Hubin-Franskin, J. Delwiche, H. Lefebvre-Brion, and A. Giusti-Suzor, Chem. Phys. Lett. **92**, 609 (1982).
[45]C. Y. R. Wu, E. Phillips, L. C. Lee, and D. L. Judge, J. Chem. Phys. **71**, 769 (1979).
[46]A. Tabche-Fouhaile, I. Nenner, P.-M. Guyon, and J. Delwiche, J. Chem. Phys. **75**, 1129 (1981).
[47]T. Akahori, Y. Morioka, M. Watanabe, T. Hayaishi, K. Ito, and M. Nakamura, J. Phys. B **18**, 2219 (1985).
[48]F. A. Elder, D. Villarejo, and M. G. Inghram, J. Chem. Phys. **43**, 758 (1966).
[49]V. H. Dibeler and J. A. Walker, J. Opt. Soc. Am. **57**, 1007 (1967).
[50]H. Oertel, H. Schenk, and H. Baumgärtel, Chem. Phys. **46**, 251 (1980).
[51]A. Jenouvrier, B. Coquart, and M. F. Merienne, J. Quant. Spectrosc. Radiat. Transfer **36**, 349 (1986).
[52]A. S.-C. Cheung, K. Yoshino, W. H. Parkinson, S. L. Guberman, and D. E. Freeman, Planet. Space Sci. **34**, 1007 (1986).
[53]H. S. Johnston, M. Paige, and F. Yao, J. Geophys. Res. **89**, 11661 (1984).
[54]B. R. Lewis, L. Berzins, J. H. Carver, S. T. Gibson, and D. G. McCoy, J. Quant. Spectrosc. Radiat. Transfer **34**, 405 (1985).
[55]S. Ogawa and M. Ogawa, Can. J. Phys. **53**, 1845 (1975).
[56]R. H. Huebner, R. J. Celotta, S. R. Mielczarek, and C. E. Kuyatt, J. Chem. Phys. **63**, 241 (1975).
[57]A. C. Allison, S. L. Guberman, and A. Dalgarno, J. Geophys. Res. **87**, 923 (1982).
[58]G. M. Lawrence and M. J. McEwan, J. Geophys. Res. **78**, 8314 (1973).
[59]*Electron-Molecule Interactions and their Applications*, edited by L. G. Christophorou (Academic, New York, 1984), Vols. 1 and 2.
[60]*Electron-Molecule Collisions*, edited by I. Shimamura and K. Takayanagi, (Plenum, New York, 1984).
[61]*Electron Impact Ionization*, edited by T. D. Märk and G. H. Dunn (Springer, Berlin, 1985).
[62]*Swarm Studies and Inelastic Electron-Molecule Collisions*, edited by L. C. Pitchford, B. V. McKoy, A. Chutjian, and S. Trajmar (Springer, New York, 1987).
[63]R. W. Carlson, J. Chem. Phys. **60**, 2350 (1974).
[64]L. C. Lee, R. W. Carlson, D. L. Judge, and M. Ogawa, J. Chem. Phys. **61**, 3261 (1974).
[65]M. Hayashi, Nagoya University Report No. IPPJ-AM-19, 1981.
[66]E. Brüche, Ann. der Phys. **83**, 1065 (1927).
[67]C. Ramsauer and R. Kollath, Ann. der Phys. **4**, 91 (1930).
[68] G. Sunshine, B. B. Aubrey, and B. Bederson, Phys. Rev. **154**, 1 (1967).
[69]A. Salop and H. H. Nakano, Phys. Rev. A **2**, 127 (1970).
[70]R. C. Dehmel, M. A. Fineman, and D. R. Miller, Phys. Rev. A **13**, 115 (1976).
[71]G. Dalba, P. Fornasini, R. Grisenti, G. Ranieri, and A. Zecca, J. Phys. B **13**, 4695 (1980).
[72]A. Zecca, R. S. Brusa, R. Grisenti, S. Oss, and C. Szmytkowski, J. Phys. B **19**, 3353 (1986).
[73]S. Trajmar, D. C. Cartwright, and W. Williams, Phys. Rev. A **4**, 1482 (1971).
[74]S. Trajmar, W. Williams, and A. Kuppermann, J. Chem. Phys. **56**, 3759 (1972).
[75]F. Linder and H. Schmidt, Z. Naturforsch Teil A **26**, 1617 (1971).
[76]J. P. Bromberg, J. Chem. Phys. **60**, 1717 (1974).
[77]K. Wakiya, J. Phys. B. **11**, 3913 (1978).
[78]H. Daimon, S. Hayashi, T. Kondow, and K. Kuchitsu, J. Phys. Soc. Jpn. **51**, 2641 (1982).
[79]T. W. Shyn and W. E. Sharp, Phys. Rev. A **26**, 1369 (1982).
[80]S. A. Lawton and A. V. Phelps, J. Chem. Phys. **69**, 1055 (1978).
[81]D. Smith and A. G. Dean, J. Phys. B **8**, 997 (1975).
[82]G. Parlant and F. Fiquet-Fayard, J. Phys. B **9**, 1617 (1976).
[83]S. F. Wong, M. J. W. Boness, and G. J. Schulz, Phys. Rev. Lett. **31**, 969 (1973).
[84]M. Tronc and R. Azria, in Symposium on Electron-Molecule Collisions, Invited Papers, edited by I. Shimamura and M. Matsuzawa, 1979, p. 105.
[85]S. Chung and C. C. Lin, Phys. Rev. A **21**, 1075 (1980).
[86]K. Wakiya, J. Phys. B **11**, 3931 (1978).
[87]C. J. Noble and P. G. Burke, J. Phys. B **19**, L35 (1986).
[88]D. Teillet-Billy, L. Malegat, and J. P. Gauyacq, J. Phys. B **20**, 3201 (1987).
[89]J. P. Gauyacq, D. Teillet–Billy, L. Malegat, R. Abouaf, and C. Benoit, in *XV ICPEAC Abstracts of Contributed Papers*, edited by J. Geddes, H. B. Gilbody, A. E. Kingston, C. J. Latimer, and H. J. R. Walters (North–Holland, Amsterdam, 1987), p. 313.
[90]B. Eliasson and U. Kogelschatz, J. Phys. B **19**, 1241 (1986).
[91]J. M. Ajello and B. Franklin, J. Chem. Phys. **82**, 2519 (1985).
[92]M. B. Schulman, F. A. Sharpton, S. Chung, C. C. Lin, and L. W. Anderson, Phys. Rev. A **32**, 2100 (1985).
[93]E. C. Zipf, J. Phys. B **19**, 2199 (1986).
[94]J. M. Ajello, J. Chem. Phys. **55**, 3156 (1971).
[95]E. C. Zipf, in *Electron-Molecule Interactions and their Applications*, edited by L. G. Christophorou (Academic, New York, 1984), Vol. 1, p. 335.
[96]L. M. Branscomb, in *Atomic and Molecular Processes*, edited by D. R. Bates (Academic, New York, 1962), p. 100.
[97]L. G. Christophorou, Radiat. Phys. Chem. **12**, 19 (1978).
[98]G. J. Schulz, Phys. Rev. **128**, 178 (1962).
[99]D. Rapp and D. D. Briglia, J. Chem. Phys. **43**, 1480 (1965).
[100]Y. Hatano, in *Electronic and Atomic Collisions*, edited by D. C. Lorents, W. E. Meyerhof, and J. R. Peterson (North–Holland, Amsterdam 1986), p. 153.
[101]H. Shimamori and R. W. Fessenden, J. Chem. Phys. **74**, 453 (1981).
[102]M. Toriumi and Y. Hatano, J. Chem. Phys. **82**, 254 (1985).
[103]Y. Hatano and H. Shimamori, in *Electron and Ion Swarms*, edited by L. G. Christophorou (Pergamon, New York, 1981), p. 103.
[104]T. D. Märk, K. Leiter, W. Ritter, and A. Stamatovic, Phys. Rev. Lett. **55**, 2559 (1985).
[105]A. Stamatovic, in *Electronic and Atomic Collisions*, edited by H. B. Gilbody, W. R. Newell, F.H. Read, and A. C. H. Smith (North–Holland, Amsterdam, 1988), p. 729.
[106]D. Spence and G. J. Schulz, Phys. Rev. **5**, 724 (1972).
[107]D. Rapp and P. Englander-Golden, J. Chem. Phys. **43**, 1464 (1965).
[108]F. J. de Heer and M. Inokuti, in *Electron Impact Ionization*, edited by T. D. Märk and G. H. Dunn (Springer, Berlin, 1985), p. 232.
[109]T. D. Märk, J. Chem. Phys. **63**, 3731 (1975).
[110]D. Rapp, P. Englander-Golden, and D. D. Briglia, J. Chem. Phys. **42**, 4081 (1965).
[111]W. L. Borst and E. C. Zipf, Phys. Rev. A **1**, 1410 (1970).
[112]J. F. M. Aarts and F. J. de Heer, Physica **52**, 45 (1971).
[113]J. F. M. Aarts and F. J. de Heer, Physica **56**, 294 (1971).
[114]J. W. McConkey and J. M. Woolsey, J. Phys. B **2**, 529 (1969).
[115]P. M. Borell, P. Borell, and D. A. Ramsay, Can J. Phys. **64**, 721 (1986).
[116]B. Coquart and D. A. Ramsay, Can. J. Phys. **64**, 726 (1986).
[117]D. A. Ramsay, Can. J. Phys. **64**, 717 (1986).
[118]R. D. Hudson and V. L. Carter, J. Opt. Soc. Am. **58**, 1621 (1968).
[119]V. Degen and R. W. Nicholls, J. Phys. B **2**, 1240 (1969).
[120]V. Hasson, R. W. Nicholls, and V. Degen, J. Phys. B **3**, 1192 (1970).
[121]V. Hasson and R. W. Nicholls, J. Phys. B **4**, 1778 (1971).
[122]G. D. Zeiss, Wm. J. Meath, J. C. F. MacDonald, and D. J. Dawson, Can. J. Phys. **55**, 2080 (1977).
[123]L. C. Lee, T. G. Slanger, G. Black, and R. L. Sharpless, J. Chem. Phys. **67**, 5602 (1977).
[124]G. M. Lawrence, Phys. Rev. A **2**, 397 (1970).
[125]C. B. Opal, E. C. Beaty, and W. K. Peterson, At. Data **4**, 209 (1972).
[126]D. T. Stewart and E. Gabathuler, Proc. Phys. Soc. **72**, 287 (1958).